Review

Antimicrobial activity of photocatalysts: Fundamentals, mechanisms, kinetics and recent advances

Priyanka Ganguly[a,b], Ciara Byrne[a,b], Ailish Breen[a,b], Suresh C. Pillai[a,b,*]

[a] Nanotechnology and Bio-Engineering Research Group, Department of Environmental Science, School of Science, Institute of Technology Sligo, Ash Lane, Sligo, Ireland
[b] Centre for Precision Engineering, Materials and Manufacturing Research (PEM), Institute of Technology Sligo, Ash Lane, Sligo, Ireland

ARTICLE INFO

ABSTRACT

Photocatalysis has recently been emerged as an effective green solution for antimicrobial disinfection applications. Photocatalytic disinfection has been observed to be efficient in deactivation of extensive varieties of organisms. Numerous gram positive and gram negative bacterial strains such as *Escherichia coli, Staphylococcus aureus, Streptococcus pneumonia etc.* have been studied. Similarly, fungal strains such as *Aspergillus niger, Fusarium graminearum,* algal (*Tetraselmis suecica, Amphidinium carterae etc.*) and viral strains have also been examined in the last decades. The present review sketches the photocatalytic mechanism and provides a brief account of several model organisms used for the disinfection studies. It presents an overview of the major kinetic models such as the Chick's model, Chick-Watson model, delayed Chick-Watson model and Hom's with modified Hom's model. Furthermore, it summarises the importance of operational parameters on the inactivation kinetics and discusses the recent advances of the disinfection results by novel composites and progress in structural or morphological improvements in conventional catalyst. The current review presents a brief overview of the state of the art commercial products utilising photocatalytic antibacterial property. Finally, it details the major international testing standards (ISO, JIS, CEN and ASTM) for photocatalytic antimicrobial applications.

1. Introduction

The access to fresh drinking water and sanitation is going to be an imperative aspect for the human sustainability in the forthcoming years [1,2]. Approximately one-sixth of the human population lacks access to safe drinking water, which causes the death of millions of people, especially children [3–5]. Apart from drinking water, the surge in the death count due to healthcare associated infections (HCAIs) is becoming a grave concern [6–9]. A study by from World Health Organization (WHO) reported that out of 100 hospitalised patients, 7 patients in developed countries and 10 in developing countries acquire a form of HCAI [10]. This endemic problem has caused fatality of about a million people last year around the globe [11,12]. The rapid transmission of the mutant antibiotic resistant strains such as *Methicillin Resistant Staphylococcus aureus* (MRSA) and *Clostridium difficile* (*C. diff*) through hospital amenities and personal care products have, necessarily evolved into an uncontrollable problem [13–16]. Therefore, the search for novel antimicrobial materials in form of colloids or surface coatings with appreciable inactivation rate and stability is a key requisite. The use of photocatalysts as potential antimicrobial agents has been studied from

the early 1990's. Matsunaga et al. were among the pioneers to exploit the use of a photocatalysts titanium dioxide (TiO_2) for potential inactivation of bacteria [17]. In a similar account, several conventional and non-conventional catalysts were also utilised and evaluated for their antimicrobial efficiency [18–21]. Photocatalysis has been widely exploited to overcome several environmental challenges posed in modern society [22–26]. The use of light to cause potential degradation and even complete demineralization is a lucrative strategy for a green alternative [27,28]. Despite the remarkable technological advancements observed in the past decade, there still exists challenges and limitations that need to be addressed. The existing research output does not qualify for high throughput processes. However, studies detailing the structural and chemical modifications for optimum band gap, and even the search for novel low band gap photocatalysts is still in progress [29–34].

The present review aims to provide a glimpse into the basic photocatalytic mechanism and offers a brief account of several model organisms used for the disinfection studies. Moreover, the review attempts to discuss the major kinetic models along with the factors influencing the inactivation kinetics. Moreover, it discusses the recent

* Corresponding author at: Nanotechnology and Bio-Engineering Research Group, Department of Environmental Science School of Science, Institute of Technology Sligo, Ash Lane, Sligo, Ireland.
E-mail address: pillai.suresh@itsligo.ie (S.C. Pillai).
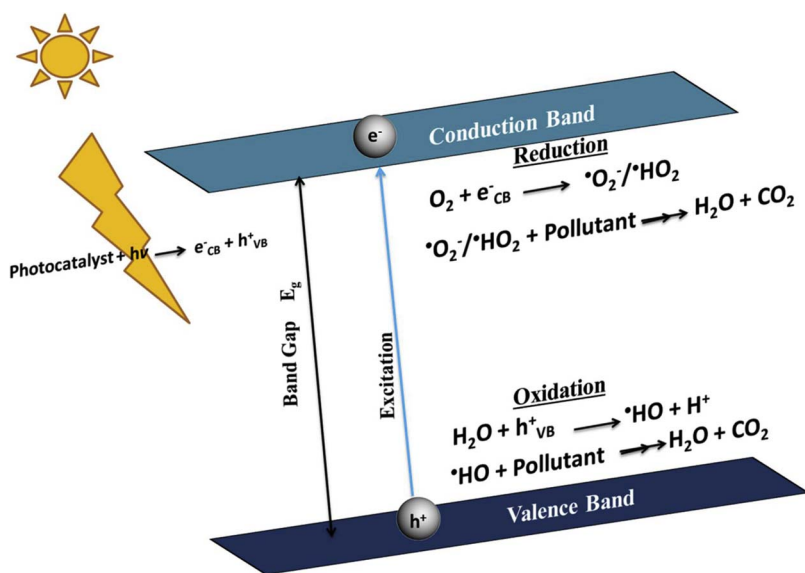
advances in disinfection process by few novel composites and details few of the structural and morphological modifications in conventional catalysts. Finally, it highlights the testing standards generally used and impart a summarised glance of the several commercial products utilising photocatalytic antimicrobial property.

2. Fundamentals of photocatalysis

Photocatalysis was first discovered over 90 years ago, however it only obtained significant interest only after the discovery of photocatalytic splitting of water by Fujishima and Honda in 1972 [35–39]. Since then, extensive studies into photocatalysis and improving the efficiency of photocatalysts has been performed [36].

Light is used to initiate the photocatalysis by bombarding photons on the surface of the photocatalyst [36,40]. Irradiation of light with compatible wavelength (greater than the band gap of the photocatalytic material) on the photocatalytic surface excites the electrons (e^-) from the conduction band of the photocatalyst, see Fig. 1 [38,40,41]. When the e^- leaves the valence band and is absorbed onto the conduction band (e_{CB}^-), a positive hole is formed on valence band (h_{VB}^+) (Eq. (1) and Fig. 1) [41–44].

$$Photocatalyst + h\nu \rightarrow h_{VB}^+ + e_{CB}^- \qquad (1)$$

In the conduction band (e_{CB}^-), the e^- reacts with oxygen ($\cdot O_2$) and it leads to the formation of superoxide radicals ($\cdot O_2^-$), or hydroperoxide radicals ($\cdot HO_2$) (Fig. 1 and Eq. (2)) [42,45,46]. The pollutants are photodegraded by the ROS into water (H_2O) and carbon dioxide (CO_2) [47,48]. Further degradation can occur by using the superoxide radicals [49]. Simultaneously, at the positive hole (h_{VB}^+) the oxidation of water takes place [42]. The oxidation reaction generates hydroxyl radicals (OH) and hydrogen ions (H^+) (Eq. (3)) [42]. H_2O and CO_2 are formed when the pollutants react with the hydroxyl radicals.

$$e_{CB}^- + O_2 \rightarrow {}^\circ O_2^- \qquad (2)$$

$$h_{VB}^+ + H_2O \rightarrow {}^\circ OH + H^+ \qquad (3)$$

While the exact mechanism of photocatalysis may vary slightly depending on the materials used and the pollutants being examined, the technology generally follows a redox reaction of electrons and holes [51–54]. Fig. 2 shows the possible pathways taken during photocatalysis inside and on the surface of TiO_2. The photocatalysis process begins on the surface of a semiconductor when photons are absorbed [50,51,54–58]. The electrons from the valence band (VB) become 'excited' from these photon to the conduction band (CB) when the energy

is higher than that of the band gap. The photocatalytic reaction is shown in Fig. 1 while Fig. 2 shows the time scale that this reaction occurs. Spectroscopic analysis, such as transient absorption (TA) spectroscopy, transient diffuse reflectance (TDR) spectroscopy, and time-resolved microwave conductivity (TMRC) measurements can be used to detect photogenerated charge carriers [54,55,59–70]. These instruments use the fact that electron-hole pairs absorb light in the visible and near IR regions and free electrons absorbs light in the IR or microwave regions [54,60,71–76].

Serpone et al. examined TA analysis for TiO_2 sols that had been 'excited' by 30-ps-width UV laser [61]. Based on the spectra from a 30 ps laser pulse, they concluded the time for trapping electrons and holes should take approx. ≤ 1–10 ps [61]. In 2001, Yang et al. examined TiO_2 nanoparticles using femtosecond TA spectroscopy and proposed that hole trapping takes ~ 50 fs and electron trapping takes ~ 260 fs [54,77]. They found that the time from inside the TiO_2 nanoparticle to the surface was 40 times quicker for the hole than the electron [54,77]. The transient adsorption of TiO_2 nanoporous film between 400 and 2500 nm was studied by Yoshihara et al. [60]. They studied a TiO_2 film that had been dipped into N_2-saturated deuterated water that had been 'excited' by low intensity pulse laser. This allowed less than one electron-hole pair to be generated per particle. This allowed the study to be performed closed to real photocatalytic conditions [54,60]. They found that it had a recombination rate is ca. 1 ms [60]. This is a much slower rate than previous studies (10 ns) that used high power laser pulses [23,54,69,70,76]. However, this result is similar to those gained from Peiro et al. and Yamakata et al. [55,78]. Later, Tamaki et al. studied nanoporous TiO_2 films for the electron-hole trapping [79,80]. They found that it took 100 fs to generate trapped electrons-holes that were shallow in depth, while it took 150 fs and 200 fs for deeply trapped electrons and holes, respectively [79,80]. Tamaki et al. stated that it took 100 ps for trapped holes to go from shallow to deep traps and that it took the electrons 500 ps to go from the shallow traps to the deep traps. They concluded that the electrons-holes should be trapped and not free charge carriers [54,79,80].

Yamakata et al. used time-resolved infrared absorption to examine the decay of free electrons prompted by water and oxygen environments [67]. They found with P25 TiO_2, the oxygen captured the electrons and there was increase of the decay rate of 10–100 μs, while in less than 2 μs there was a reaction between the water vapour and the holes [54,67]. Furube et al. examined the charge recombination kinetics for Pt/TiO_2 and found that on top of finding the normal charge recombination there was a new decay component (a few ps) when
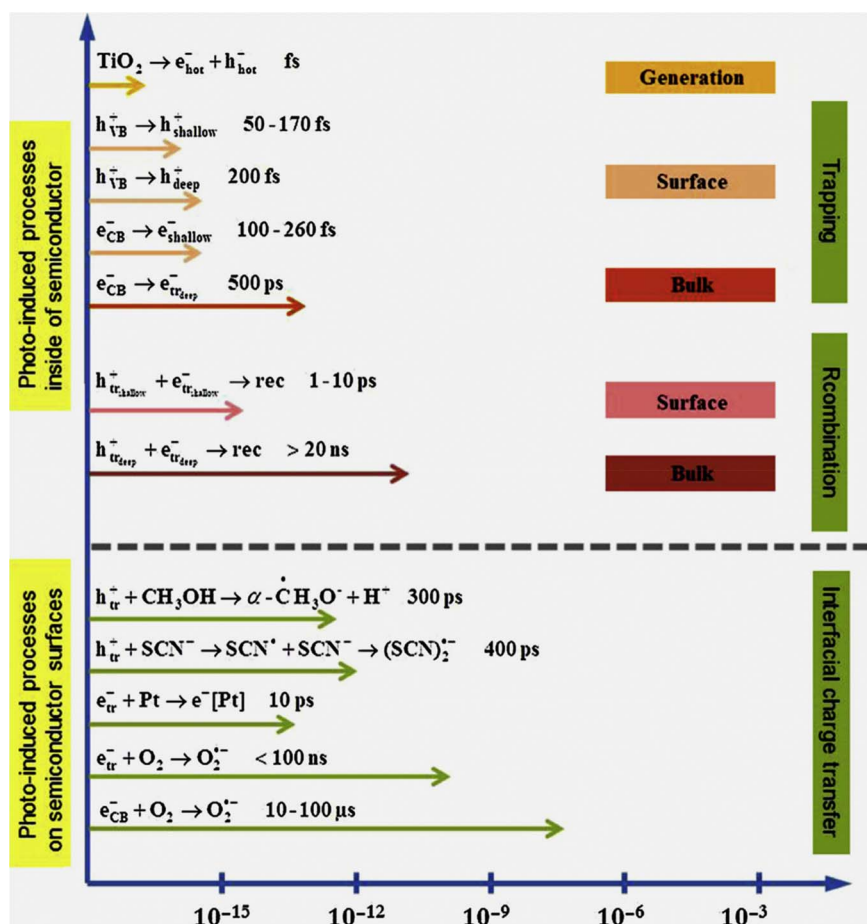
Fig. 2. Steps of the TiO_2 photocatalysis process [50,51]. Reprinted with permission of Etacheri et al. Full details are given in the respective publication.

exited at 390 nm. They found that the higher amount of Pt present, the more it effected the migration of electrons [67]. They determined the migration of the electrons between TiO_2 and Pt caused the increase in the decay process [54,67]. Iwata et al. also examined the decay process with Pt-TiO_2. As with Furube et al., Iwata et al. also stated that the electrons are transferring from TiO_2 and Pt and the found the decay rate of 2.3 ps [66]. They propose that a small portion of the electrons remain on TiO_2 as there is still signal present after some time (100 s of ps) [54,66].

Fujishima and Zhang proposed three points based on the research examined. Firstly, they speculated that the recombination during photocatalysis is a slow process as a result of efficient charge trapping [54]. Secondly, they speculated that the charge transfer process competes with charge recombination [54]. Finally, they concluded that it can take μs to ms for photocatalysis to occur once the electron-hole pair created. This suggests that under low-intensity UV irradiation (1 mW cm^{-2}, ~1015 photons s^{-1} cm^{-2}), the electron-hole pair are generated and has already gone through reaction or charge recombination before a photon is absorbed by the photocatalyst [54].

Recent studies have examined the ability of a photocatalyst to utilise visible light or natural light [38]. There has also been increasing investigations into non-titania photocatalysts [38,81–88]. Most of these were first examined for photocatalytic water splitting but have now been examined for a number of other applications such as water/air treatment [38]. Due to the vast volume of studies examining photocatalysts, they have been divided into two categories; oxide photocatalysts and non-oxide photocatalysts (Fig. 3). How the valance and conduction bands are affected by the change in pH is one of the major differences between the two categories [38,81–83].

Using two photocatalysts to form heterojunctions has also been examined in recent years [38]. The e$^-$ are transferred between the two photocatalysts, this reduces or stops recombination [38]. This increases the charge separation and affects the rate of photodegradation [38,89].

It has been reported that the rate of photocatalytic degradation is completely depended on surface coverage of the photocatalyst by the contaminates being examined [90,91]. This applies to the photocatalytic inactivation of micro-organisms. In order to have an effective rate of photoinactivation the micro-organisms must have surface interactions with the photocatalyst [91]. The reactive oxygen species (ROS) generated during photocatalysis will first damage the cell wall of the micro-organisms [91,92]. The ROS first breaks down the lipopolysaccharide layer of the cell wall; this then leads to the attack of the peptidoglycan layer, peroxidation of the lipid membrane and oxidation on the proteins membrane [91,92]. The damage to these layers causes the potassium ions from the bacterial cells to leak, which affects the cell viability. This leakage leads to the loss of crucial cell functions and ultimately cell death [91,92].

3. Structure of microorganisms

Photocatalysis has been utilised as a vital tool in developing potential disinfection strategies against several hostile microorganisms [93]. There exists numerous bacteria, viruses, fungi, protozoa *etc.* in a water source [94,95]. These microorganisms existing in the water source are very complex in nature. Hence it is very important to understand the microbial morphology, which can render information to enable photocatalytic advances for disinfection applications [96–98].

3.1. Bacteria

Bacteria are single-celled, prokaryotic organisms which can flourish in various and sometimes harsh conditions such as in a desert, inside
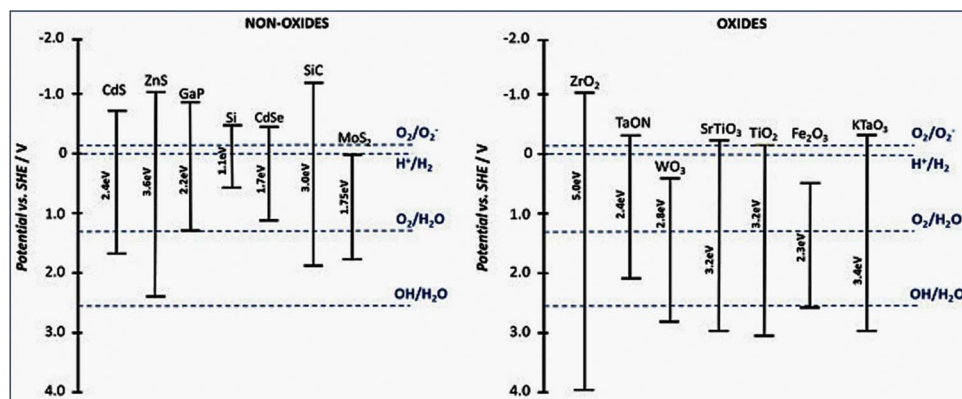
Fig. 3. The band gaps of non-oxide photocatalysts (left) and oxide photocatalysts at a pH of 7 (right). Reprinted with permission of Waldmann et al. Full details are given in the respective publication [38,81–83].
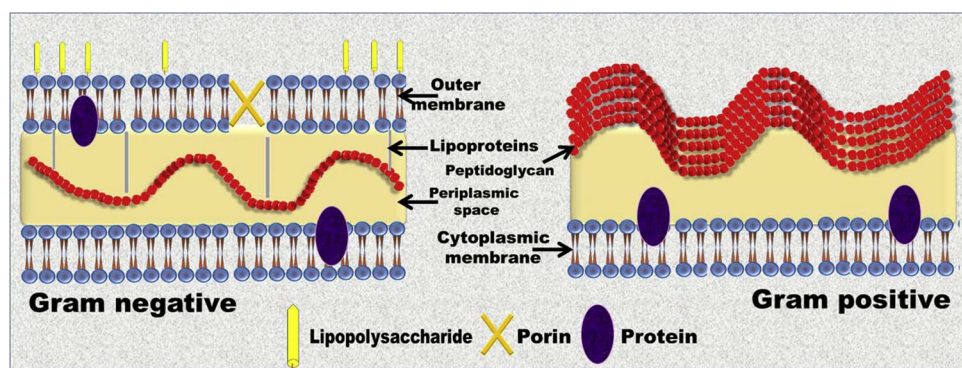

Fig. 4. Schematic diagram illustrating the difference in the bacterial cell wall composition.

soil or in the sea [99–103]. The bacterial body has very minimalistic organelles devoid of any compartments, which support the basic functions [104–106]. The nuclear material has no definitive boundaries and thus floats in the cytoplasm [107,108]. There exist different types of bacteria and they are classified based on two aspects, their shape and the constituent of the cell wall [109]. According to the cellular wall composition the bacteria are classified as Gram-positive and Gram-negative bacteria (Fig. 4) [110–112]. The purple gram stain on the cell walls of the bacteria signifies the presence of single peptidoglycan polymer layer, which accounts for about 80% of the cell wall composition and the rest accounts for fats and lipid. These bacteria are known as gram-positive bacteria; they have a classical cell wall thickness of 20–80 nm. They do not have the lipopolysaccharide layer but have a single layer of phospholipid. The gram-negative bacteria emit a red stain and their cell wall has only 10% of peptidoglycan. These bacterial cells are made up of 2 layers of phospholipid and a layer of lipopolysaccharide. These cell wall layers promote selective permeability in many cases [113,114]. Bacteria are the most common model organism studied to understand the disinfection mechanism and to evaluate the photocatalytic efficiency of the composite [87–89].

3.2. Fungi

Fungi are eukaryotic cells with the complex cellular organisation [115]. The fungal cells have compartmentalised organelles (mitochondria, Golgi apparatus etc.) which are responsible for normal cellular function [116]. The fungi have rigid cell walls made up of polysaccharides called chitin (Fig. 5) [117,118]. The complex cell wall structure helps them to survive in extremely harsh conditions [119–121].

3.3. Viruses

Viruses are unicellular organisms that are smaller than the bacteria, which fail to thrive in the absence of host material [123–125]. The capsid, a protein chain that provides protection from extremely harsh environments and they also act as a site for binding into the host body [126,127]. Viruses attach onto the host cell's surface by recognising these binding receptors and inserting its genetic material inside the host body [128–131]. Thus the cell surface receptor site of any host and the binding site of the viruses are the key element for the entry route of these viruses [132]. The manipulation of the structure of the binding site can deactivate the growth of the viruses. Photocatalytic disinfection can prove to be an effective tool to destruct these binding sites by the ROS production.

3.4. Algae

Algae are a complex group of organisms [133,134]. They exist in different sizes, from micron size to few meters in length, as in the case of seaweeds [135–137]. The lack of roots and vascular tubes make them distinct from plants [138–140]. Apart from the beneficial effect of algae for CO_2 fixation, the extensive growth of microalgae leads to the production of toxins and results in harmful consequences for the marine life and humans [141,142]. This effect is widely known as the algal boom and considered as a major concern for water treatment plants [143–145].

4. Photocatalytic disinfection mechanisms of microorganisms

The understanding of the bacterial inactivation process is important to underlay the effective development of novel composites for photocatalytic disinfection mechanisms [146,147]. Matsunaga et al. were the first to demonstrate the light induced inactivation process and proposed that the degradation of Coenzyme A by potential ROS generated in the reaction process as the likely mechanism for bactericidal activity. The denaturation of the enzyme resulted in possible inhibition of respiratory activity, which further led to the cause of death [17]. However, researchers soon found that the cell death was prompted by the disruption of the cell wall membrane. Leakage of potassium ions and the
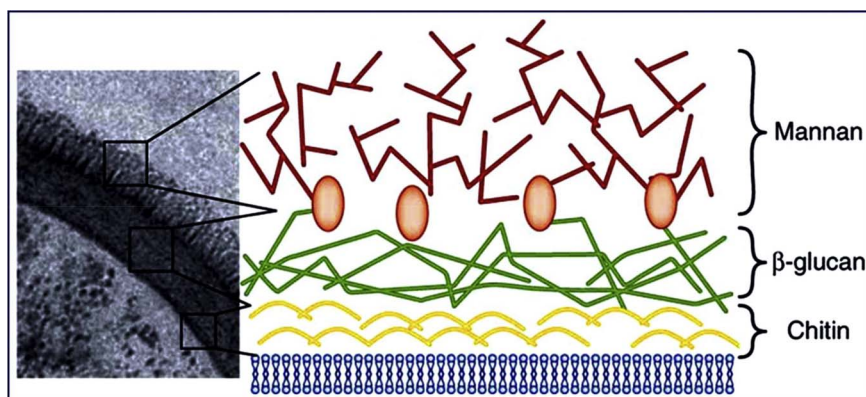
Fig. 5. Electron micrograph of the fungal cell wall (*C. albicans*), with carbohydrate-rich layers of the fungal cell wall, highlighted: mannan (mannosylated proteins), β-glucan and chitin. Reprinted with permission of Hardison et al. Full details are given in the respective publication [122].
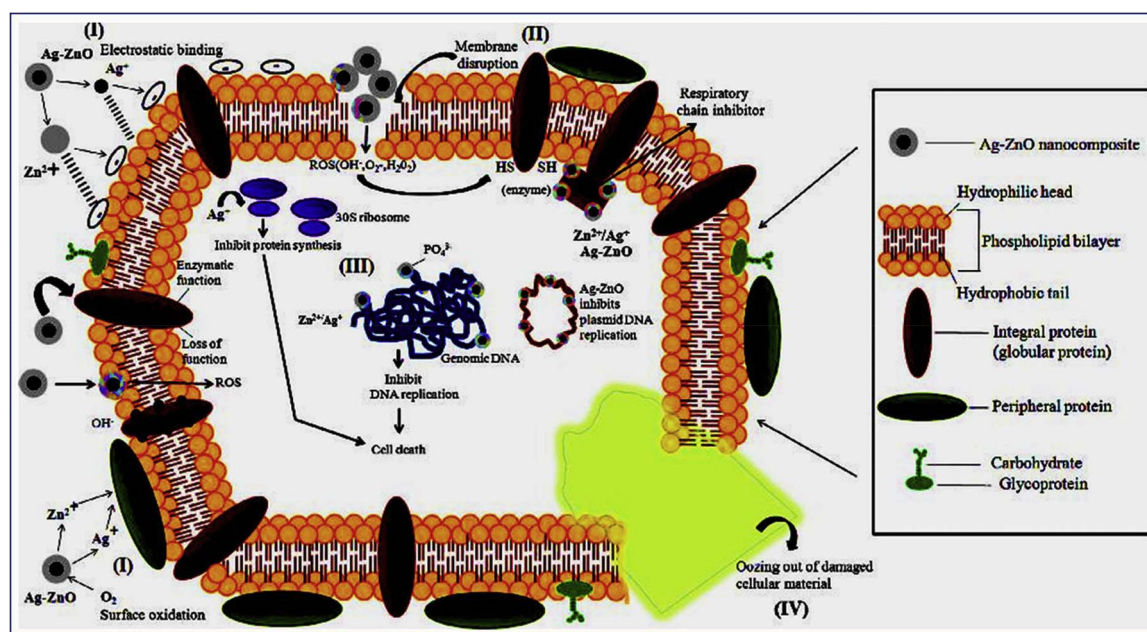

Fig. 6. Schematic representation of antibacterial mechanism of Ag–ZnO nanocomposite. Reprinted with permission of Matai et al. Full details are given in the respective publication [157].

subsequent flow of cellular components such as RNA and protein resulted in complete destruction of these cells. Saito et al. were among the first to confront these results, the Transmission Electron Microscopy (TEM) images illustrated the complete destruction of these cells [148]. Kikuchi et al. evaluated the role of the ROS in the reaction process, by the addition of hydroxyl radical scavenger. It was observed that the bactericidal activity was reduced by the addition of the scavenger but the activity did not cease. The authors proposed that the presence of the more reactive hydrogen peroxide as the reason of continued bactericidal activity. Hence the antimicrobial activity is a cooperative effect of all the ROS intermediates formed in the reaction process [149]. Advances in defining the plausible mechanism for photocatalytic disinfection of microbes led researchers to understand the reasons for the destruction of the cell wall. Jacoby et al. finally found the evidence of complete mineralisation of the damaged cells. The Scanning Electron Microscopy (SEM) micrographs were used to observe the disappearing colonies of bacteria and ^{14}C radioisotope labelling was used to analyse the carbon content [150]. Manes et al. found that the peroxidation of the phospholipid component of the cellular wall due to the potential ROS attack leads to its disruption [151]. Furthermore, Sokmen et al. quantified the lipid peroxidation by quantifying the formation of Malondialdehyde. The by-products of lipid peroxidation were reported at a very early stage. It was found that the continuous irradiation resulted in complete degradation of Malondialdehyde into simpler products like

Carbon Dioxide (CO_2) and water (H_2O) [152]. The formations of these by-products were monitored by Gas chromatography mass spectrometry (GC/MS) [153]. Later Kiwi et al. investigated the peroxidation mechanism of the bacterial cell wall on the TiO_2 surface. The cell wall destruction mechanism was monitored by Fourier Transform Infrared spectroscopy with an Attenuated Total Reflection accessory (FTIR-ATR). The h$^+$ formed in the reaction process competes with the oxidation of the lipid polysaccharide layer or the recombination reaction of h$^+$ and e$^-$, the authors claims this as the first step towards the complete disintegration process [154].

Remy et al. investigated the bacterial targets and assessed the bacterial cultivability along with its cell wall integrity under dark and visible light irradiation. The authors found that the titania particles exhibited potential bactericidal behaviour way before the light irradiation. The increase in titania content decreased the bacterial cells cultivability. The particles caused damage to cell wall integrity which further contributed to the increased bactericidal nature. On the other hand, the cell wall permeability was not affected in the presence of silica nanoparticles. The electrostatic charge difference between the particles and the cell wall was found to be the prime reason. In a more deeper understanding, the RNA and the DNA of the bacterial cells were found to be the bacterial targets of the oxidative attacks induced by the ROS generated during the photocatalytic disinfection mechanism [155]. Wang et al. investigated the dominant ROS responsible for the

Table 1
Summarised analysis of the plausible mechanisms defined in recent years.

Mechanism Defined	Reference
Degradation of Coenzyme A	Matsunaga et al. [17]
Disruption of the cell wall membrane observed in TEM images	Saito et al. [148]
Production of H_2O_2	Kikuchi et al. [149]
SEM micrographs and C^{14}labelling to illustrate the disappearing colonies	Jacoby et al. [150]
Peroxidation of the phospholipid component of the cellular wall	Manes et al. [151]
Quantified the lipid peroxidation by measuring the Malondialdehyde formed	Sokmen et al. [153]
Defined the toxic nature of the nanoparticles and found the nuclear material as the potential targets of the bactericidal function.	Remy et al. [155]
Identified the influential ROS species and found hydroxyl radicals as a prominent contributor	Wang et al. [156]

visible light induced disinfection mechanism against *E. coli* using B and Ni co-doped titania microspheres. The hydrogen peroxide (H_2O_2) generated in the system was identified to be the most predominant species. The hydroxyl radical present in the bulk solution and on the surface of the catalyst contributed to the H_2O_2 production [156]. Matai et al. studied the antibacterial mechanism of Ag-ZnO composite and effectively defined plausible routes of inactivation (Fig. 6).

The first route depicted is the direct interaction of the composite with the bacterial cell. This could happen by the surface oxidation which will result in the dissolution of the Ag and Zn ions. The possible interaction might also be attained by direct contact of the composite particles with the bacterial cell wall by electrostatic interaction. The second possible method is by the disruption of the bacterial cell wall by potential ions or attack by the ROS generated. The third way of inactivation is the alteration/inhibition of the DNA replication by the interaction of the ions or the ROS with sugar-phosphate groups causing gene alteration, thus altering the protein expression responsible for cellular functioning. Finally, the potential disruption of the membrane leads to the release of the intracellular materials, which eventually leads to cell lysis [157]. Table 1 provides a summarised glimpse of the mechanisms defined to access the antimicrobial behaviour of the photocatalyst.

5. Kinetics

5.1. Photocatalytic kinetics

Chemical kinetics is essential in understanding the rate and the factors influencing the chemical process to attain equilibrium at any given amount of time [158]. A rise in interest over heterogeneous photocatalysis has ensued to several reports on different kinetic models [159].

5.1.1. Langmuir-Hinshelwood (L-H model)

Photocatalysis as a heterogeneous catalysis was always explained using the classical L-H model [56,160,161]. It is based on the assumptions that the adsorption of the reactants occurs on the catalyst surface [23,56]. The reaction proceeds between the adsorbed species and later the products desorb from the surface [56]. Herman et al. in a significant contribution have tried to explain several myths related to photocatalysis and he also explained this model in a more generalised approach, taking into the account to the several changes made to this model to result into a modified L-H model [158,162,163]. In a bimolecular reaction;

$$A + B \rightarrow C + D \tag{4}$$

The rate of the chemical process is proportional to the surface coverage (Θ) of the reactant

$$r = k\theta_A\theta_B \tag{5}$$

Where the coverage Θ_i varies as;

$$\theta_i = \frac{K_iX_i}{1 + K_iX_i} \tag{6}$$

Where $K_i \rightarrow$ adsorption constant (in dark), $X_i \rightarrow$ concentration in liquid phase or partial pressure P_i in gas phase

Hence Eq. (5) becomes;

$$r = \frac{kK_AK_BX_AX_B}{(1 + K_AX_A)(1 + K_BX_B)} \tag{7}$$

$k \rightarrow$ true rate constant

Generally, one of the two reactants for example A would have high concentration and the other reactant B shall have low concentration. Therefore, the change in concentration of A remains constant, since its small consumption makes negligible change in concentration [158,163].

Therefore, Eq. (5) reduces to

$$r = k'\theta_B \tag{8}$$

[where K′ = KΘ_A]

k'→ pseudo true rate constant

$$\Rightarrow r = \frac{k'K_BX_B}{(1 + K_BX_B)} \tag{9}$$

(as shown in Fig. 7)

Hence,

If; X = $X_{max} \Rightarrow \Theta_B$ = 1

Therefore, Eq. (9) reduces to r = k′

Or if; X<< $X_{max} \Rightarrow \theta_B = \frac{K_BX_B}{(1 + K_BX_B)} \approx K_BX_B$

Therefore, Eq. (9) reduces to

$$r = k'K_BX_B = k_{App}X_B \tag{10}$$

$k_{App} \rightarrow$ Apparent first order constant

5.1.2. Direct-indirect model (D-I model)

Satoca et al. introduced an alternative kinetic approach, the "Direct–Indirect" (D–I) model [164]. The model proposes several major
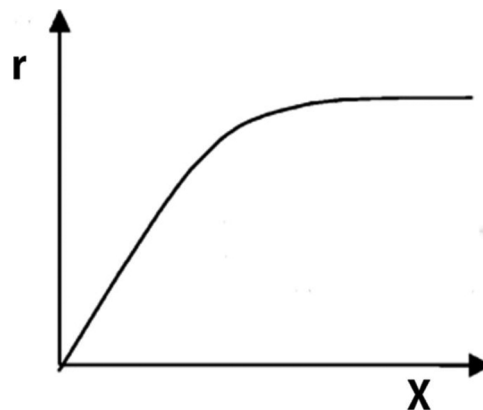
Fig. 7. Langmuir- Hinshelwood model. Variation of photocatalytic kinetics (r) in due influence of the catalyst concentration (X).

concepts on direct, indirect, adiabatic and inelastic interfacial transfer of charge, which further establishes a physical meaning to the kinetic parameters involved. The L-H model discusses the kinetics of the reaction in an equilibrated adsorption/desorption of reactants on the surface of the semiconductor material under a constant illumination. Moreover, it also fails to establish a meaningful relationship between the incoming radiant flux (Φ) and the reactant concentration (X). However, the present model furnishes a functional dependence of the photooxidation rate (r) on the experimental parameters (photon flux and pollutant concentration).

The rate of photooxidation depends on all the interfacial charge transfer and the reaction between the conduction band electrons with the dissolved O_2 to form potential reactive species, is certainly the rate determining step amongst all of them [165]. However, the discussion stumbles upon the debate on the participation of photogenerated valence band holes (h_f^+) in a direct reaction (DT) with organic substrate or transfer via an indirect transfer (IT) mechanism by utilising hydroxyl radicals (surface trapped holes h_s^+). The brief number of possible routes of direct and indirect transfer is:
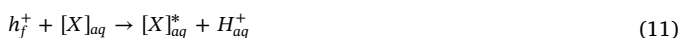
$$h_f^+ + [X]_{aq} \rightarrow [X]_{aq}^* + H_{aq}^+ \tag{11}$$

Photogenerated holes reacting with reactants in the aqueous solution (not absorbed on the catalyst surface).

$$h_f^+ + [X]_s \rightarrow [X]_s^* + H_{aq}^+ \tag{12}$$

Photogenerated holes reacting with reactants absorbed on the catalyst surface.

$$h_s^+ + [X]_{aq} \rightarrow [X]_{aq}^* + H_{aq}^+ \tag{13}$$

Surface trapped holes reacting with reactants in the aqueous solution (not absorbed on the catalyst surface).

$$h_s^+ + [X]_s \rightarrow [X]_s^* + H_{aq}^+ \tag{14}$$

Surface trapped holes reacting with reactants absorbed on the catalyst surface.

When the organic molecules are not adsorbed on the catalyst surface, the hole transfer between the reactants in the aqueous solution occurs adiabatically. Marcus developed a Fluctuating Energy Level Model which defines this transfer mechanism and later Gerischer interpreted it on the semiconductor electrolyte interface [166–168]. This model helps in predicting a hole transfer rate constant (k_{ox}^{adb})

$$k_{ox}^{adb} \propto exp\left[\frac{-(E_{red} - E_s)^2}{4\lambda kT}\right] \tag{15}$$

Where, $E_s \rightarrow$ Energy of the surface trapped holes, $E_{red} \rightarrow$ The most probable energy of the occupied energy levels of reactants in the aqueous solution, $\lambda \rightarrow$ The reorganisation energy (between 0.5–1.0 eV).

However, under strong interaction which increases the competitive adsorption between the reactant molecules and the water molecules. In such case, the hole transfer mechanism is not adiabatic but inelastic and is not governed by this model anymore. Thus the modified rate constant (k_{ox}^{ins}) is;

$$k_{ox}^{ins} \propto \sigma\hat{c} \tag{16}$$

Where, $\sigma \rightarrow$ Hole capture cross-section of filled surface states, $\hat{c} \rightarrow$ Thermal velocity of free hole.

The direct transfer mechanism of holes is largely predominated than indirect mechanism, but on the other hand indirect mechanism is the only transfer process available in the absence of specific adsorption.

The L-H model is based on the equilibrated adsorption of the reactants, hence in a Langmuir type adsorption isotherm the relationship between the concentration of dissolved and adsorbed species is given as;

$$[X]_s = \frac{ab[X]_{aq}}{1 + a[X]_{aq}} \tag{17}$$

Where, a → adsorption constant, b → desorption constant.

However, in this model the author's utilises Ollis et al. idea of non-equilibrated adsorption of the reactants. Ollis proposes a pseudo-steady-state analysis for reaction, in the event of tampered adsorption–desorption equilibrium under illumination conditions. In this case, the adsorbed species are attacked by the photogenerated valence band free holes through an inelastic direct transfer process [158]. So according to pseudo-steady-state approach proposed by Ollis, the surface coverage (Θ_A) of a reactant say A, assuming that $\frac{d\theta_A}{dt} = 0$, then;

$$\frac{d\theta_A}{dt} = [X]_{aq}k_1(1 - \theta_A) - k_{-1}\theta_A - k_{ox}^d[h_f^+]\theta_A = 0 \tag{18}$$

Where, k_1 and k_{-1} are the adsorption and the desorption constant, thus Eq. (17) reduces to

$$[X]_s = \frac{ab[X]_{aq}}{1 + a\left\{[X]_{aq} + \left(\left(\frac{k_{ox}^d}{k_{-1}}\right)\left(\frac{k_0'}{k_1[O_s^{2-}]} + k_{ox}^d[X]_s\right)\right)\right\}} \tag{19}$$

Thus, Eq. (19) defines that the concentration of the reactant adsorbed on the catalyst surface decreases with the increasing radiant flux [169]. Apart from this D-T model, there were several other improvements suggested but none turned out to be influential as both these models [170–174]. Salvador et al. strongly suggested that the formation of free hydroxyl radicals only by the reaction of dissolved O_2 with electron and dismissed the notion of earlier models of their participation of photogenerated holes. Mills et al. in a more recent review describes effectively the contradiction to this same argument and provides a summarised outlook of all such recent approaches. Hence, the discussion of kinetics revolves around the formation of hydroxyl radicals, their possible route of formation and above all their impact on reactant surface [164,172,175].

5.2. Disinfection kinetic models

The kinetic modelling of any chemical reaction aids in understanding the key elements responsible for the reaction [176–178]. The photocatalytic disinfection process is a very complex phenomenon. It involves multiple factors for example pH of the sample, different catalyst loading, irradiation intensity, turbidity, the temperature of the reaction mixture and most importantly the complex structure of the microorganism [179,180]. The presence of different strains of microorganisms, various target organs inside their body and finally the mineralisation of the target component are among the few key factors governing the kinetic process. The model helps to simplify the complicated reaction phases into simpler mathematical expression [181,182]. The kinetic models portray survival curves, a graphical illustration signifying the semilog plot of inactivation on contact time. The variation in the shape of the survival curves plays a crucial factor in the assessment of the mechanism of microbial inactivation [183]. Fig. 8 shows the different survival curves observed in general. Curve (a) in Fig. 8 exhibits a first order kinetics of inactivation, which illustrates the exponential death of microbes with time. Curve (b) in Fig. 8 displays an exponential disinfection but shows a shoulder initially, which implies the delay in diffusion of the disinfectant molecules to the sites of action. Curve (c) in Fig. 8 shows a curve of a shoulder and a tailing off, while Curve (d) is only limited by having a tailing off sequence at the end of the curve. The presence of several families of microbes in the sample with varying degree of resistance causes a decrease in the rate of inactivation, which results in the tailing off nature [179,183–186].

The kinetic inactivation models are derived based on the following assumptions:(a) uniform distribution of microorganisms and the disinfectant molecules. (b) constant pH, temperature and the concentration of the catalyst (disinfectant). (c) adequate mixing to evade liquid
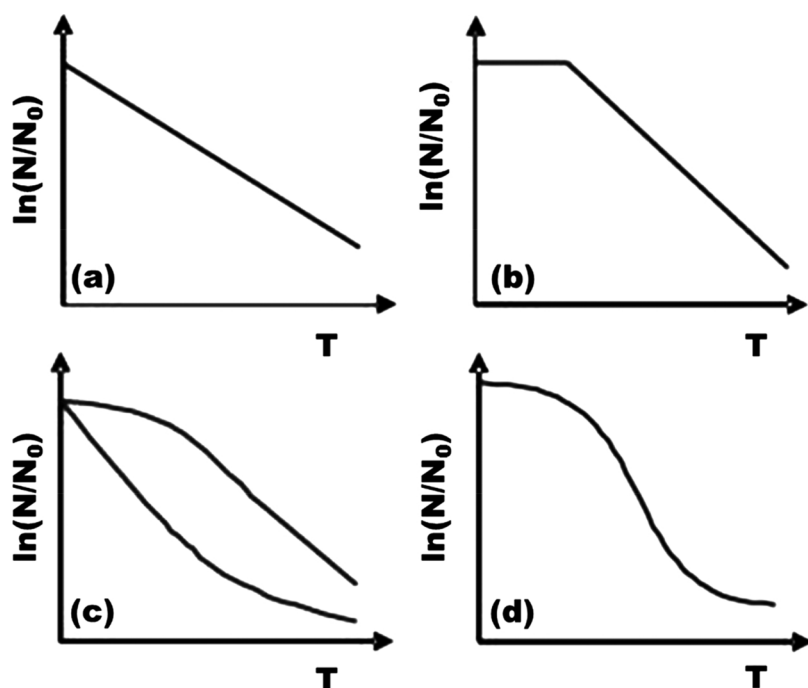
Fig. 8. Survival curves observed for different kinetic models used in the photocatalytic disinfection. Curve (a) first order kinetics of inactivation, illustrates the exponential death of microbes with time, Curve (b) exponential disinfection but with a shoulder initially, Curve (c) curve with a shoulder and a tailing off, and Curve (d) curve with a tailing off sequence at the end. Reprinted with permission of Marugan et al. Full details are given in the respective publication [188].

diffusion as a potential limiting agent in the chemical reaction [179]. There exist four common kinetic models; (1) Chick's model, (2) Chick-Watson model, (3) Delayed Chick-Watson model, (4) Hom model. The general expression of the differential rate law used by these kinetic models is as (Eq. (20)) [179,183–186];

$$\frac{dN}{dt} = -KmN^xC^nt^{m-1} \tag{20}$$

Where; $\frac{dN}{dt}$ = Rate of inactivation, N = Number of survivors at contact time t, K = Reaction rate constant, C = Concentration of the disinfectant, m, n, x = Empirical constants.

5.2.1. Chick's model

Chick's paper on "The laws of disinfection" in 1908 compared the bacterial inactivation to a chemical reaction, where individual bacteria was considered as molecules [187].

$$xN + nC \xrightarrow{K_1} S\,(dead\ microorganisms) \tag{21}$$
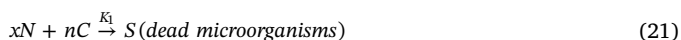
The rate of reaction for the following reaction is given as [188];

$$\frac{dN}{dt} = -K_1N^xC^n(dead\ \ microorganisms)^S \tag{22}$$

Here x and n = 1 and considering the reaction is irreversible, thus S = 0. Hence Eq. (22) results in

$$\frac{dN}{dt} = -K^*N \tag{23}$$

Where K* is considered as the pseudo first order rate constant where K* = K_1C. Thus Eq. (23) is the generalised rate law expression of Chick's law. It states that the rate of inactivation is proportional to the number of surviving microbes at a constant disinfectant concentration (Fig. 8(a)).

Integration of Eq. (23) results in;

$$ln\frac{N}{N_0} = -K^*T \tag{24}$$

Where N_0 = Initial microbial population.

In a more recent assessment, Danae and Dionissios explain the importance of the true order of this kinetic model [178]. The authors explain that the reaction parameters such as temperature, catalyst concentration *etc.* are accounted as a constant termed as pseudo- first order constant. Hence, at different N_0 values, but a constant experimental setup should render constant K* value. If the value remains constant, then indeed it could be termed as a first order constant. The authors also explained the importance of ROS concentration in the reaction mixture. The ROS in the reaction mixture is a predominant factor governing the rate of disinfection; hence the 'N' value cannot alone be considered as an exclusive factor. The excess of ROS will potentially cause quicker disinfection and display a first order kinetics, meanwhile, a low ROS concentration will turn into a potential limiting agent in the disinfection process. Therefore, ROS in the disinfection process is certainly a principal factor governing the kinetics of the process. Moreover, the ROS produced in the reaction depends on the constant experimental factors Thus the experimental parameters are the true controller of the disinfection kinetics [179,189,190].

5.2.2. Chick-Watson model

The Chick's law assumes first-order kinetics and in most instances, the microbial inactivation does not follow this assumption. Watson in the same year modified the chick's law by incorporating the concentration-time product which considers the effect of varying concentration of disinfectant (Eq. (25))[187]

$$K = C^nT \tag{25}$$

Where 'K' is a constant for a microbe and a set of conditions. 'n' is a constant and 'T' is the time required to attain a certain activation point. An n value less than 1 signifies the increased importance of the contact time, more than the disinfectant concentration. The addition of Watson's function in Chick's law results in a Chick-Watson pseudo first order rate law as [187,191]:

$$\frac{dN}{dt} = -KNC^n \tag{26}$$

Where K is the first order rate constant. Integration of the above expression results in (Fig. 8 (a)) [187,191].

$$ln\frac{N}{N_0} = -KC^nT \tag{27}$$

$$\frac{N}{N_0} = e^{-KC^nT} \tag{28}$$

5.2.3. Delayed Chick-Watson model

The simplified nature of the Chick-Watson model makes it equitable in most studies. However, the Chick-Watson model has its own pitfalls, it assumes that the microbes are of single strain and the inactivation occurs on a single hit and at a single spot. It shows neither the initial shoulder (lag phase) nor the tailing off nature. The delayed Chick-Watson model introduces a time lag parameter to overcome the shoulder observed in the disinfection process (Fig. 8(b)) [192–195].

$$\frac{N}{N_0} = \begin{cases} 1, & T \leq T_{lag} \\ e^{-KC^n T}, & T > T_{lag} \end{cases} \tag{29}$$

5.2.4. Hom's and modified Hom's model

The delayed Chick-Watson model can represent the shoulder or the tailing off at a time but the concurrent presence of both cannot be expressed using this model. The Hom's disinfection model proposed in 1972 provides a generalised expression for the time-concentration product. It is very similar to the Chick-Watson model, an addition of a power factor m for time is observed. When $m = 1$, the equation reduces to the Chick- Watson model, $m > 1$ results in the appearance of the initial shoulder in the curves, while $m < 1$ lead to the appearance of the tailing off (Fig. 8 (c)). Hence the Hom's model also does not allow the occurrence of both the initial lag and the tailing off in the curve at the same time [188,196,197].

$$ln\frac{N}{N_0} = -KC^n T^m \tag{30}$$

Thereafter a modification is introduced in the Hom's model which allows the presence of the initial lag, the log- linear phase and the tailing off at the end of the curve. The modified Hom's model is as (Fig. 8(d)) [188,196,197]:

$$ln\frac{N}{N_0} = -K_1[1 - \exp(-K_2 T)]^{K_3} \tag{31}$$

Where K_1, K_2, K_3 are the empirical constants in this model.

In a more recent study by Marugan et al. the authors evaluate the photocatalytic disinfection of *E. coli* using a simplified kinetic model having 3 parameters; kinetic constant (k), pseudo adsorption constant (K) and inhibition coefficient (n). This model takes into account of the 3 different phases (the initial lag phase, log-linear phase and the tailing off nature) in the survival curve [198].

Thus, the bacterial cell reduction is expressed as a function of the log of the relative cell population and the function of time. The reduction parameter defines the decrease of the levels of microbes in the samples by factors of 10, which is easily converted into percentage (%) expression. Hence a 1-log reduction signifies a death of 90%, 2-log reduction indicates a death of 99% and 3-log reduction implies a death of 99.9% of the microbes [199].

6. Factors influencing the disinfection mechanism

There exist several reports detailing the impact of the operational parameters (Fig. 9) of the disinfection mechanism but on a noteworthy contribution, Rincon et al. were among the first researchers to study the effect of these factors on the inactivation process [200–204].

6.1. pH and catalyst loading

The effect of pH in the photocatalytic process is crucial [205]. The change in the pH value modulates the effective charge of the reaction mixture. The industrial waste water streams has very extreme pH levels and hence variations of the disinfection activity in different pH values need to be cognisant of this. The surface charge of the catalyst and its microbial cell wall is dependent on the overall pH of the system.

Moreover, the arrangement of the band structure and the size of the catalyst aggregates depend on this operating parameter. The surface charge of the catalyst or the disinfectant and the pH has a defined correlation. The pH value at which the surface charge of the catalyst surface is zero (point of zero charge) is known as the isoelectric point. Understanding of the operational parameters and the plausible disinfection mechanism is governed by this isoelectric point and the pH of the disinfection mixture. The positive surface charge of the catalyst attracts to the negatively charged cell wall structure of the microbes. This subsequently increases the disinfection process. Watts et al. found that the bactericidal property remained unaltered between the pH of 5 and 8 [199]. But conversely, Herrera et al. observed that the rate of disinfection process was improved in TiO$_2$ based system at pH 5 [206]. Improved activity was observed in the presence of TiO$_2$ and not just by acidification of the cells. There also exist several reports illustrating the non-dependence of pH in the disinfection process [194].

Catalyst loading is another important operating parameter of concern. It has been observed in several studies that the disinfection process improves with an increase in the catalyst concentration. However, it rapidly reaches a saturation limit, where the rate of the reaction remains constant even with the increase in the catalyst concentration. The increase in the catalyst concentration eventually leads to turbidity and hinders the absorption of the incoming radiation. Studies have been performed to optimise the mass of the catalyst required for the specific disinfection process, to avoid excess usage [207–211].

6.2. Irradiation length and intensity

There exist several reports, elucidating the difference in the inactivation activity in the absence and presence of disinfectant and additionally in the exposure of with or without irradiation exposure [212–214]. Rincon et al. also studied the influence of irradiation time and intensity for bacterial inactivation in the presence and absence of light. In the absence of titania, the samples were irradiated for different time intervals [202]. Bacterial inactivation occurred as long as the irradiation continued but the viability numbers soon reached to initial values, when they were placed in the dark. The same set of samples was evaluated in presence of titania and was irradiated for different time interval. The inactivation was effective and remained constant even in dark. It was observed that a continuous irradiation without any interruption allowed the complete disinfection but an interrupted irradiation reduced the bactericidal activity. It is understood that the self-defence mechanisms of the bacteria help them to recover. The bacterial cell generates superoxide dismutase (SOD) enzyme as a defensive mechanism to cope with the disproportionate amount of ROS inside the cell and reduces the oxidative stress. Howbeit, the ROS eventually generated in the presence of the catalyst on due irradiation of light is significantly high which ultimately leads to complete bacterial disinfection. The results obtained from this study are quite contradictory to other results available. It was observed that the intermittent illumination increased the bacterial inactivation. Hence, the influence of continuous and intermittent irradiation depends on the type of microorganism [215]. Similarly, Li et al. also observed no bactericidal activity in the *E.coli* samples in absence of any disinfectant and the rate of photocatalytic inactivation reduced as the samples with catalyst loaded were placed in the dark [216].

In a photocatalytic reaction, the irradiation intensity (ϕ) is undoubtedly a major parameter of concern [217]. The catalyst surface on being illuminated renders active sites for ROS production which further initiates the inactivation process. Higher irradiation results in increased ROS production, but in addition to the intensity of the irradiation, the surface area of the disinfectant are also a factor in the effective rate of ROS production. In a UV active semiconductor material for example TiO$_2$ the disinfection profile is limited (with a higher disinfection time) when irradiated with sunlight, as it only constitutes 4% of UV component. In such cases, the surface area of the irradiant is crucial. Studies
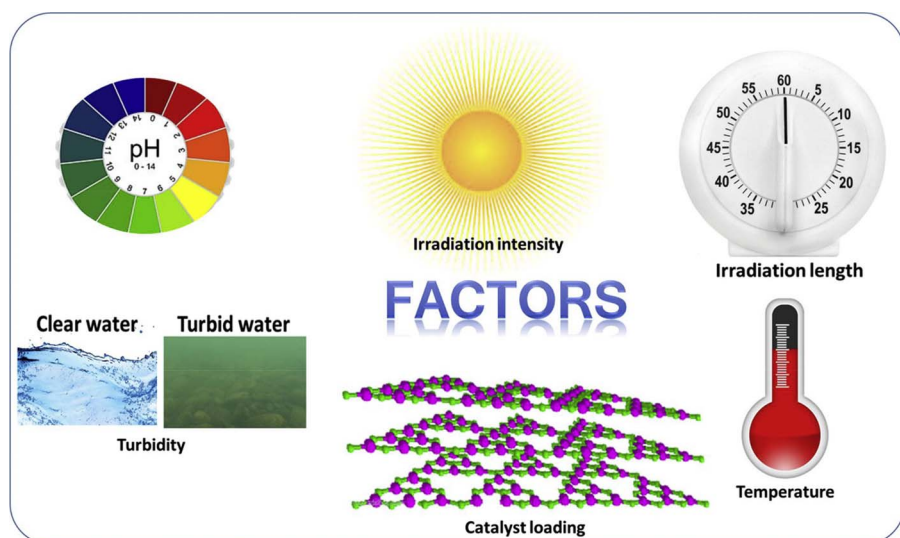
revealed an increase in the irradiation intensity enhances the effective bacterial disinfection and the inactivation continued even in dark. This residual effect is attributed to the significant quantity of ROS produced. This linear dependence of inactivation with the irradiation intensity (φ) was later modified and changed into square root dependency. Malato et al. explained the change in the dependency using the following elaborate derivation; the disinfection activity occurs in 3 definite stages [218]:
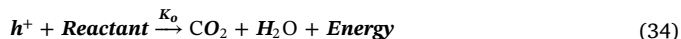
1. Formation of electron/hole pairs;

$$\textbf{Photocatalyst} + h\vartheta \xrightarrow{K_f} \textbf{e}^- + \textbf{h}^+ \tag{32}$$

2. Recombination of this pairs and;

$$\textbf{e}^- + \textbf{h}^+ \xrightarrow{K_R} \textbf{Energy} \tag{33}$$

3. Oxidation of the reactant;

$$\textbf{h}^+ + \textbf{Reactant} \xrightarrow{K_o} CO_2 + H_2O + \textbf{Energy} \tag{34}$$

In n-type photocatalysts, like Titania, the holes are found to be limited compared to the electrons (photogenerated electrons and the n-type electrons) and hence these holes turn out to be the limiting agent.

At any instant, the rate of the reaction (r):

$$r = K_0[h]Reactant \tag{35}$$

and

$$\frac{d[h]}{dt} = K_f\varphi - K_R[e][h] - K_o[h]Reactant = 0 \tag{36}$$

Therefore, for high φ values, the electron and holes generated shall have the same value and so,

$$[e][h] = [h]^2, \tag{37}$$

Thus the above equation reduces to:

$$K_f\varphi = K_R[e][h] + K_o[h]Reactant \tag{38}$$

Furthermore $K_R[h]^2 \gg K_o[h]Reactant$. Similarly, for low φ values $K_R[h]^2 \ll K_o[h]$.

Hence the summarised description of the effect of the change in the φ values is:

For high φ values;

$$K_f\varphi \approx K_R[h]^2 \rightarrow [h] \approx K_{ap}\varphi^{0.5} \tag{39}$$

$$r = K_0 K_{ap}\varphi^{0.5}Reactant \tag{40}$$

For low φ values;

$$K_f\varphi \approx K_o[h]Reactant \rightarrow [h] \approx K'_{ap}\varphi \tag{41}$$

i.e. $r = K'_{ap}\varphi Reactant$ \hfill (42)

At very high φ values,

$$r = f(\varphi^0) \tag{43}$$

In this case, the photocatalytic process depends on the mass transfer rather on the incoming irradiation and hence the rate of the reaction remains constant with the increase in the intensity of the radiation. This is attributed to several factors such as the saturation of the reactive sites on the catalyst surface, the absence of potential oxidizers or because of the presence of any unwanted organic molecules.

6.3. Temperature and turbidity

In a photocatalytic disinfection system, the temperature is not an essential factor. However, in general the photocatalytic disinfection rate decreases with the increase in operational temperature [219]. Though there exist several kinds of literature studying the effect of temperature in the inactivation process. Studies on the effect of temperature on the disinfection process are very contradictory. The thermal energy imparted to the system is not sufficient enough to overcome the band gap barrier. The trivial quantity of heat energy present in the disinfection mixture is employed in the activation process of the reactant on the catalyst surface. The activation energy required by the reactants increases at a low operational temperature and remains moderately effective in a medium temperature between 20–80 °C. In contrast, when the temperature of the system starts to increase beyond 80 °C, the adsorption of the reactants on the catalyst surface becomes deferred and increases the recombination of the charged carriers [20,218,219]. Contrary to this, there are few reports contradicting this very analysis. The authors found that increasing the temperature reduced the time for complete inactivation as the increased temperature amplified the collision frequency of the molecules and resulted in an improved reaction rate [194,220]. Overall, in photocatalytic disinfection the use of sunlight could be justified as the potential source of light and heat, this makes the process an effective alternative to the existing water treatment strategies, which consumes a fair share of energy in the heating process.

Turbidity is another key factor which affects the decontamination process. The presence of small insoluble sub-particles for example clay, planktons and microorganisms is the cause of the turbidity. The turbid water results in the attenuation of incoming light and the absorption level varies significantly. It was observed that an increased level of

turbidity in the water sample decreases the photocatalytic inactivation rate. The increased particulate level diminishes the ability of the incoming irradiation to breach through the turbid water. Moreover, the catalyst added lead to aggregation, which reduces the disinfection activity and the heat captivated in the system stimulates the bacterial growth [200,221,222].

7. Recent advances in photocatalytic disinfection

The disinfection property of various model organisms has been studied extensively using several classes of nanomaterials. Many of these materials do not compose required optical potential to necessarily initiate the inactivation process. However, in due course of time, the chemical and morphological modifications of these materials have been explored and resolved this limitation. The present section aims to provide a summary of the recent advances in photocatalytic antimicrobial studies in past few years and provides a brief description of those work.

7.1. TiO$_2$ based composites

Apart from doping of metal and non-metals in titania, composites were also explored with other materials such as C$_{70}$ (Fullerene), quaternary oxides *etc.* Etacheri et al. reported the formation of carbon-doped anatase-brookite titania nano-heterojunction. The prepared composites were studied by the inactivation of the strains of *S. aureus*. The fabricated composite exhibited exceptional antibacterial efficiency. The carbon doping in the composite resulted in the introduction of a mid-level band gap, which served as the cause for the narrowing down of the band gap of the entire composite. Moreover, the carbon dopant increased the charge separation within the composite matrix (Fig. 10) [223].

Ouyang et al. fabricated a composite of C$_{70}$ and TiO$_2$ and studied the bactericidal activity of the prepared composite on irradiation of visible light. The disinfection rate of *E. coli* tripled in this composite compared to TiO$_2$ due to the significant production of hydroxyl radicals [224]. A photoreactor device was created which consists of open-cell foam comprising a dopant metal, a dopant non-metal, titanium, and oxygen. The high surface area foam is utilised for *E. coli* disinfection and the low back pressure supports the dynamic flow applications [225]. Hu et al. fabricated of AgI/TiO$_2$ composites and evaluated the biocidal action on *E. coli* and *S. aureus*. The complete destruction of the cell membrane was observed in the TEM images and the degradation products of the bacteria were identified by FTIR [226]. The same group also reported the AgBr/TiO$_2$ composites and evaluated the biocidal action on *E. coli* and

S. aureus [227]. Reddy et al. reported the formation of Ag-TiO$_2$ composite with Hydroxyapatite. The appreciable photocatalytic behaviour of Hydroxyapatite, the bactericidal nature of Ag and the improved disinfection ability of the Ag-TiO$_2$ resulted in a total bacterial disinfection of the strains of *E. coli* within 2 min of irradiation [228]. Titania/carbon nanotube heterojunction was formed by Akhavan et al. and studied the inactivation of *E. coli* under visible light irradiation. The Ti–C and Ti–O–C carbonaceous bonds formed effectively contributed to the effective visible light absorption and eventually contributed to the enhanced disinfection [229]. Lately, Koli et al. investigated the bacterial disinfection efficiency of TiO$_2$/MWCNT (Multi-walled carbon nanotube) composite against the strains of *E. coli* and *S. aureus* under visible light irradiation. The composite showed improved disinfection compared to the TiO$_2$ samples because of the effective charge separation imposed due to the MWCNT [230]. TiO$_2$/Ag$_3$PO$_4$ heterostructure composite was investigated for fungal disinfection against the strains of *F. graminearum*. The composite prepared introduced efficient charge separation and increased the visible light absorption property. The fungal strains were effectively inactivated within 100 min of irradiation. The Equivalent Series Resistance (ESR) measurements identified the hydroxyl radicals as the major reactive oxygen species [231]. Akhavan and Ghaderilt prepared nanocomposites of TiO$_2$ and reduced graphene oxide which exhibited improved bactericidal efficiency under solar light. The improved activity was attributed to the electron sink or the electron acceptor ability of the reduced graphene oxide which effectively introduced charge separation and delayed the recombination rate [232]. Later, Liu et al. reported the formation of graphene oxide–TiO$_2$ nanorod composites, which exhibited improved *E. coli* inactivation compared to that of the titania nanorods. The improved efficiency was attributed to the cooperative effect of the two-dimensional graphene sheets deposited on the high surface area of titania nanorods [233]. In a similar attempt, Gao et al. also studied the bacterial inactivation of the strains of *E.coli* using the titania-graphene composite under visible light illumination. The graphene oxide was prepared using the Hummer's method and the composite exhibited improved inactivation compared to their parent constituents [234]. In 2015, Ibanez et al. studied the inactivation of the same composite using two different strains of bacteria (*E. coli and F. solani*) and compared the results with P25 (Standard TiO$_2$ nanoparticles with mixed anatase and rutile phase). The composites illustrated rapid disinfection compared to the inactivation results of P25 and the improved efficacy was attributed to the formation of singlet oxygen in the reaction mixture [235]. The same group in a very recent study elaborates the plausible disinfection mechanism by altering the irradiation parameter and usage of several ROS scavengers. The hydroxyl radical, singlet oxygen and hydrogen
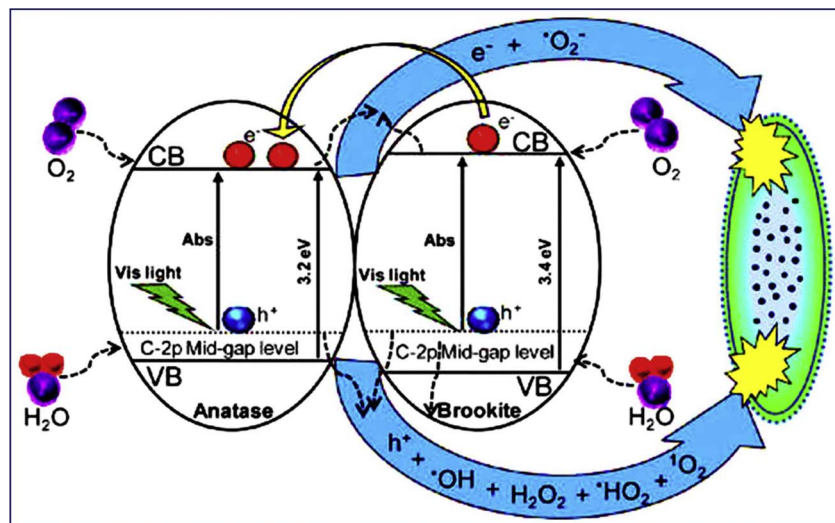

Fig. 10. Schematic illustration of the antibacterial mechanism using carbon-doped anatase-brookite heterojunctions. Reprinted with permission of Etacheri et al., American Chemical Society. Full details are given in the respective publication [223].

Table 2

Summarised results of few TiO$_2$ based binary composites against inactivation of the bacterial strains of E. coli.

Binary TiO$_2$ base composite	Light source	Inactivation time (in h)	Disinfection results	Ref
C$_{70}$/TiO$_2$	Visible light	2	73%	Ouyang et al. [224]
AgI/TiO$_2$	Visible light [2.8 mW/cm^2]	1	7.8 log	Hu et al. [226]
AgBr/TiO$_2$	Visible light [2.8 mW/cm^2]	0.6	3.2 log	Lan et al. [227]
CNT/TiO$_2$	Visible light [110 W/m^2]	1	99.8%	Akhavan et al. [229]
GO/TiO$_2$	Simulated sunlight [100 W/m^2]	0.5	8.2 log	Liu et al. [233]

peroxide were the major ROS generated, under visible light irradiation, but however, the singlet oxygen was found to be the dominant ROS [236]. Table 2 below provides a summarised glance of few reports on TiO$_2$ based composites against inactivation of the bacterial strains of *E. coli*.

Titania based visible light active coatings are also reported widely in past few years, however few reports do stand out from the crowd. In such an effort, Bai et al. reported the fabrication of transparent nanotitania coatings with enhanced antimicrobial potential (*A. niger*). The coating utilised polyhydroxy fullerene (PHF) as an enhancer for nano TiO$_2$ photocatalysis [237]. Rtimi et al. reported a pioneering result of Cu/TiO$_2$ sputtered films for bacterial inactivation. The films exhibited excellent bactericidal property even in dark. The presence of Cu ions has gradually improved the inactivation process even in low visible light irradiation. The authors monitor the copper leaching and found the levels only at ppb, which is cytotoxically safe according to human standards [238]. The same group studied the photocatalytic effect of bactericidal nature of Cu-doped TiO$_2$−ZrO$_2$ by magnetron sputtering. The inactivation enhanced up to 3 folds in case of Cu doped composite compared to bare titania and zirconia even at an extremely low copper content (0.01–0.02 wt%). The antibacterial property is prominent because of the strong affinity between the phosphate and the thiol group in the negatively charged bacterial cell wall with copper (a strong electron donor) [239]. Similarly, Wang et al. lately reported the formation of 2-D titania thin films with memory of photocatalytic activities. Upon irradiation, photogenerated electrons were produced and stored in the thin film matrix which further participated in the bacterial inactivation process in the dark (Fig. 11) [240]. Apart from titania thin

films, antimicrobial activity of titania nanotubes have also been reported. Carroll et al. investigated the bactericidal nature of the nanotubes against the strains of *E. coli, S. aureus*. The tubes showed improved inactivation (Log-2) compared to P25 under 24 h of UV irradiation. The surface hydroxyl radicals were observed to be the key participant in the inactivation process, which subsequently embarked the importance of the high aspect ratio of the nanotube [241]. In the series of doping studies, metal dopants have always been a vital candidate. Many fresh studies utilising metal dopants have emerged in past years but few of them stood out from the crowd. He et al. reported the deposition of Au nanoparticles over ZnO by photoreduction technique. A small molar% of Au enhanced the antibacterial effects by many folds. The enhanced levels of ROS produced in the disinfection process contributed to the bactericidal behaviour of the material [242]. In a similar context, Fisher and co-workers reported a Molybdenum doped titania structures which effectively inactivated brewery microorganisms. This hybrid structure showed 5- log of bacterial and 1-log of fungal inactivations. Moreover, it also exhibited dual nature of photocatalytic and antimicrobial property, since the composite caused inactivation even in dark [243]. Few reports of novel composites have also emerged in past couple of years, but the sections above had already detailed many such examples. However, few of the recent reports is briefly discussed in this section. TiO$_2$(Eu)/CuO nanocomposite was fabricated and studied for the bactericidal property against *E. faecium*. The report illustrated a selective photoactive disinfection against *E. faecium*. The selective binding of the CuO nanoparticles on the bacterial surface is considered to be the plausible reason behind the inactivation process [244]. Boron and Cerium doped titania was reported by Wang et al. and evaluated the antimicrobial efficiency against the strains of *S. aureus*. The co-doping contributed to a synergistic bactericidal property [245]. Similarly Fan et al. reported the development of Fe and N co-doped titania samples. These novel composites also demonstrated improved bactericidal behaviour over cotton fabrics. This study evidently demonstrated the self-cleaning and the antimicrobial activity of these composites for commercial applications [246]. Similarly Raut et al. also reported the fabrication of chitosan-TiO$_2$:Cu nanocomposite for biomedical applications. The resulted composite exhibited a 200% enhanced inactivation of bacterial strains of *E. coli* and *S. aureus*, compared to chitosan only inactivation samples. The plausible mechanism of the disinfection process is illustrated in Fig. 12 [247].

A ternary composite of titania nanocrystals, carbon dots and reduced graphene oxide was fabricated and evaluated for their photocatalytic disinfection ability. The electron storage ability of the graphene reduced the formation of superoxide radicals in the binary composites of TiO$_2$ and graphene. The addition of carbon dots improved the charge separation and contributed to the delayed recombination ability, which consequently resulted in improved
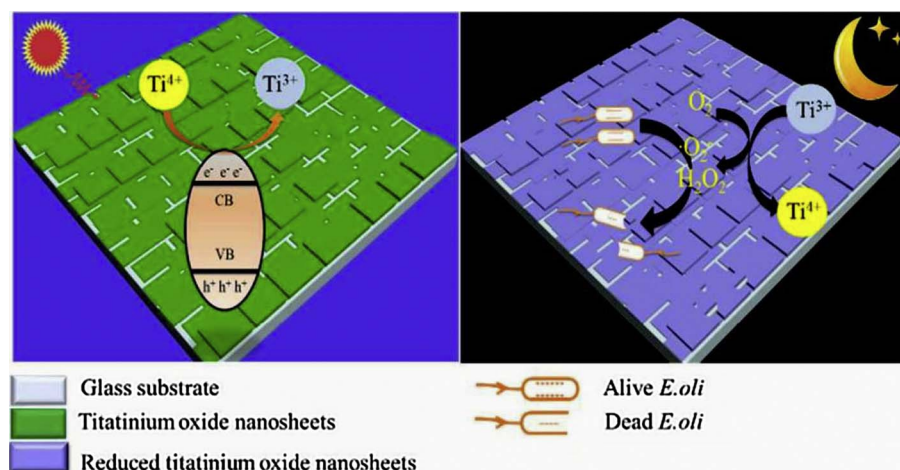

Fig. 11. Schematic illustration of the antibacterial mechanism on the titania nanosheets. Reprinted with the permission of Wang et al. Full details are given in the respective publication [240].
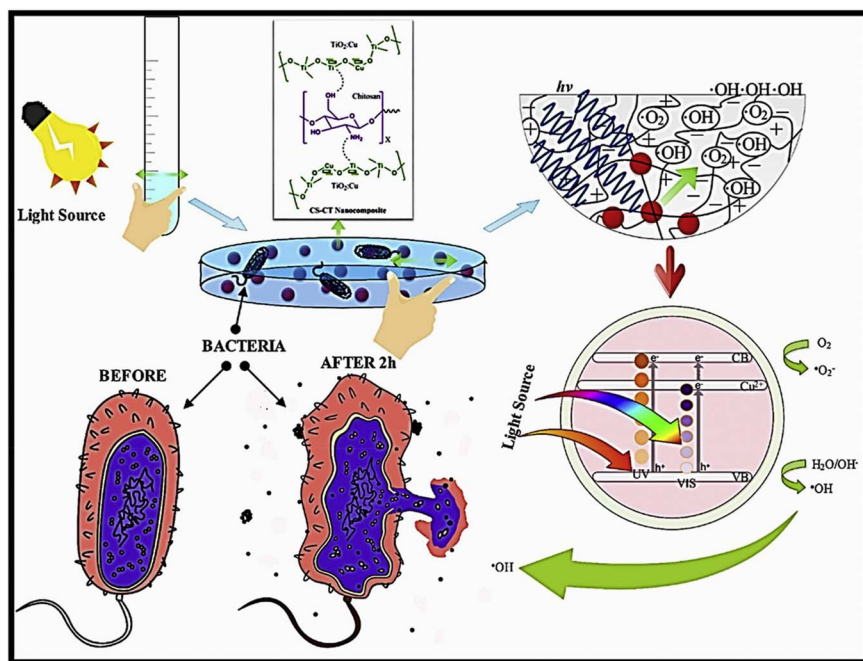
Fig. 12. Illustration of the plausible mechanism of antimicrobial activity in the presence of nanocomposite. Reprinted with permission of Raut et al. Full details are given in the respective publication [247].
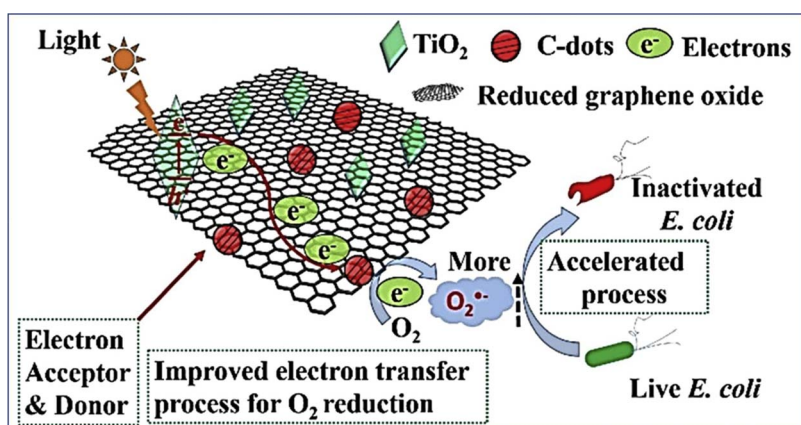

Fig. 13. Schematic illustration of the plausible disinfection mechanism using the ternary composite of TiO$_2$, carbon dots on reduced graphene oxide. Reprinted with permission of Zeng et al.. Full details are given in the respective publication [248].

bactericidal efficiency (Fig. 13) [248]. Similarly, a novel composite film of P/Ag/Ag$_2$O/Ag$_3$PO$_4$/TiO$_2$ was reported for bacterial inactivation. The film exhibited 100% sterilisation within 5 min of irradiation. Photogenerated holes and superoxide radicals were found to be the active reactive oxygen species responsible for the appreciable efficacy [249].

7.2. Magnetic composites

The recyclability and the recovery of the catalysts has always been the challenging factor [250]. The fabrication of magnetic photocatalysts has resolved this issue up to a certain extent. The magnetic core accelerates the disinfection rate and helps in quick retrieval. The metal ions (Fe/Ni etc.) cause leaching from the composite which necessarily tamper the bacterial cell wall. Moreover, these metal ions fasten the inter charge transfer within the composite structure and subsequently delays the recombination rate and effectively contributes to the enhanced inactivation kinetics [251]. The use of these magnetic photocatalysts for light induced microbial disinfection is very limited. Rana and Rawat et al. synthesised composites of nickel ferrite with titania which has appreciable magnetic and photocatalytic property. The magnetic core helps in the easy recovery of the catalyst and the titania shell emanates its photocatalytic behaviour. The composite derived

showed an efficient antibacterial effect against the strains of *E. coli* [252,253]. In a more recent effort Wai et al. fabricated a magnetic composite of Fe$_2$O$_3$-AgBr and studied its bactericidal efficiency. The as prepared composites showed improved antibacterial effect under high temperature and alkaline pH [254]. Chen et al. fabricated a hybrid ternary composite of Ce/N co-doped TiO$_2$/NiFe$_2$O$_4$/diatomite. The hybrid catalyst features multifunctional purposes. The presence of diatomite increases the adsorption pattern and the Ce/N co-doped TiO$_2$ escalates the visible light absorption behaviour. Moreover, the presence of NiFe$_2$O$_4$ aids the magnetic recyclability of the catalyst. The composite exhibited ferromagnetic nature and thus can be easily separated using an external magnet, which subsequently improves the recyclability efficiency of the catalyst (Fig. 14(a)). The scavenger study helped in detecting the predominant ROS (superoxide radical) responsible for the bacterial inactivation of the strains of *E. coli* and define a plausible mechanism (Fig. 14(b)) [255].

7.3. Bismuth-based composites

The search for visible light active heterogeneous photocatalysts led researchers to stumble upon several new classes of compounds [256]. Bismuth-based composites are among such new class of materials possessing appreciable narrow band gap and thus illustrating improved
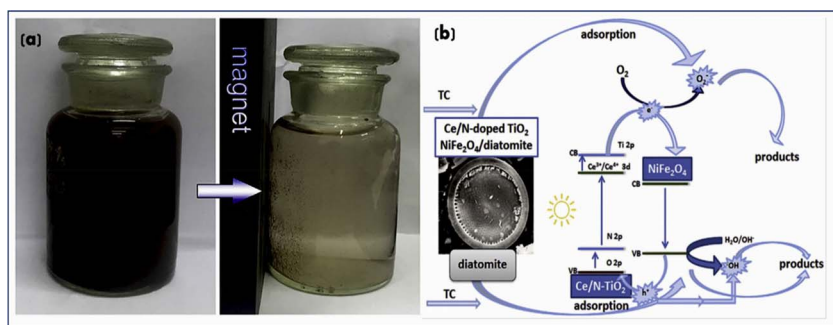
Fig. 14. (a) Catalyst solution before and after separation (b) Photocatalytic mechanism of producing potential ROS. Reprinted with permission of Chen et al. Full details are given in the respective publication [255].
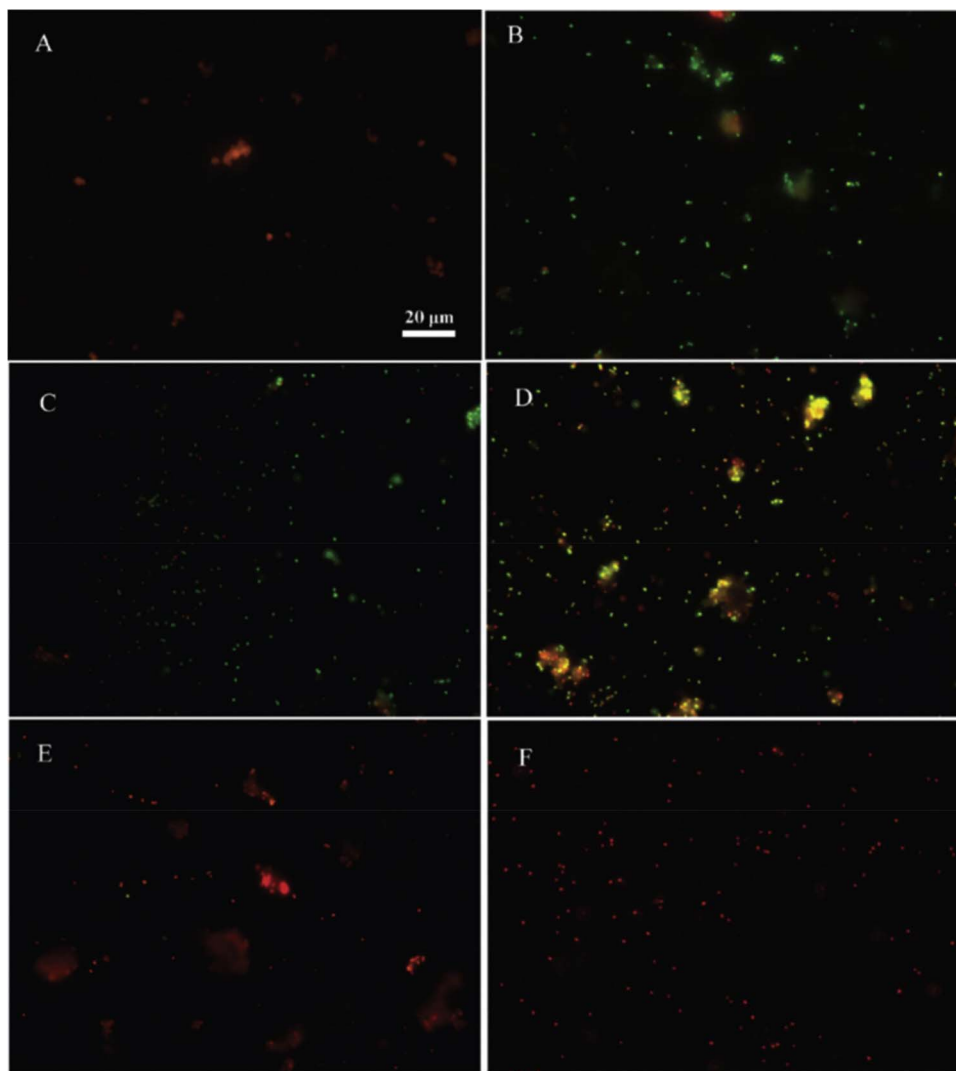

Fig. 15. Fluorescence microscopic images of (A) Only AgBr-Ag-Bi$_2$WO$_6$ nanojunction, (B) The mixture of photocatalyst and E. coli K-12 before irradiation, and after irradiation by VL for (C) 1, (D) 2, (E) 5, and (F) 10 min. Reprinted with permission of Zhang et al. AMERICAN CHEMICAL SOCIETY. Full details are given in the respective publication [262].

visible light absorption compared to the conventional photocatalysts such as TiO$_2$ and ZnO [257,258]. The photocatalytic bacterial inactivation ability of Bi$_2$WO$_6$ and its composites of Ag were studied by Ren et al.[259] The inactivation of the bacterial strains by Bi$_2$WO$_6$ followed a first order kinetics and the TEM images illustrated the complete destruction of the bacterial cells [260]. On the other hand, the Ag composites also illustrated enhanced bactericidal nature due to the synergistic effect between the noble metal and the semiconductor material [261]. In a more profound effort, a new composite of Ag-Br − Ag − Bi$_2$WO$_6$ was developed and the bactericidal nature of the composites was studied under visible light irradiation (Fig. 15). The resulted composite showed efficient inactivation compared to the other

binary composites. The bacterial cell destruction was observed in the TEM images and validated again by the release of the potassium ions [262]. In a more notable contribution, Alfaro and co-workers have studied the algal disinfection effect using different metal oxides. Binary oxides for example Bi$_2$MoO$_6$, Bi$_2$WO$_6$ and Bi$_2$W$_2$O$_9$ were evaluated for their photocatalytic efficiency. The combined effect of the UV radiation and the photocatalysts showed the disinfection of algae *A. carterae* within 30 min and *T. suecica* in 60 min [263].

Qin et al. reported Nanospheres of bismuth oxides and investigated for the bacterial inactivation of *S. aureus* and *E. coli*. The Nanospheres caused significant inactivation under visible light irradiation [264]. Wang et al. reported the formation of a novel visible light active
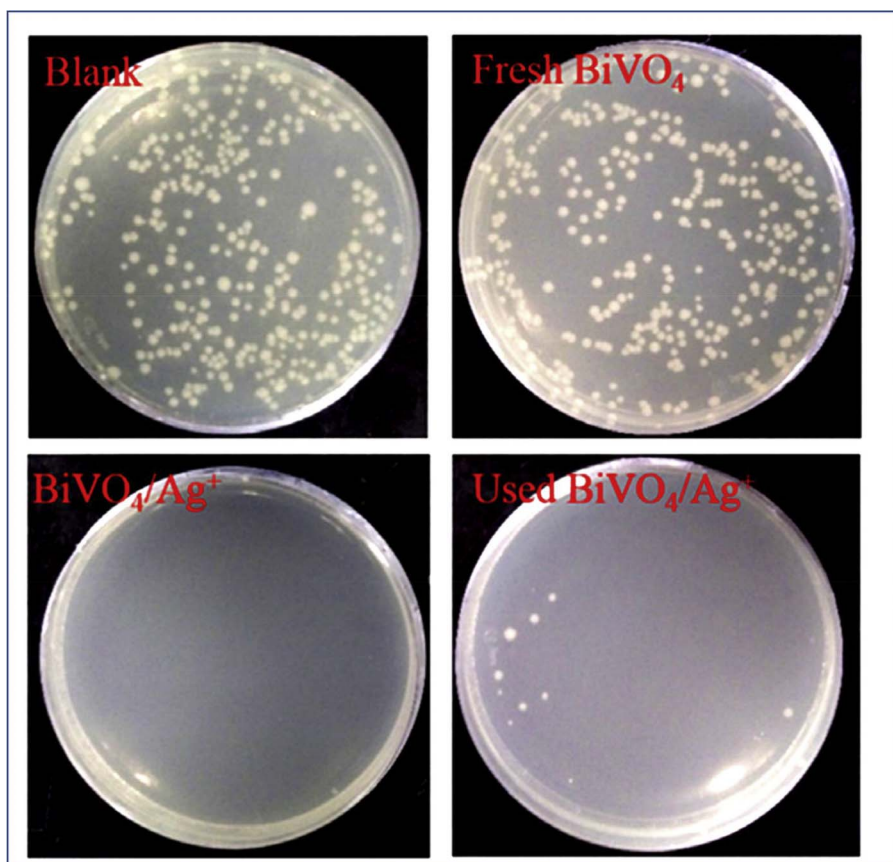
Fig. 16. *E. coli* colonies on an agar plate in the presence of blank, fresh BiVO$_4$, BiVO$_4$/Ag+, and used BiVO$_4$/Ag$^+$ under visible light irradiation for 60 min. Reprinted with permission of Huang et al. Full details are given in the respective publication [276].

photocatalyst, monoclinic dibismuth tetraoxide (m-Bi$_2$O$_4$) with a narrow band gap of 2 eV. The composite was further exploited for its potential bactericidal nature and showed complete inactivation within 120 min of visible light irradiation. The Mott-Schottky plots from the impedance measurement found the hydroxyl radicals as the major ROS responsible for the different photocatalytic disinfection mechanism [265]. Bismuth Oxyhalide has been an interesting choice of material for visible light photocatalysis. The layered tetragonal matlockite structure of BiOX (X = Cl, Br, I), characterised by [Bi$_2$O$_2$]$^{2+}$ slabs interweaved by double slabs of halogen atoms contributes to the narrow band gap nature. Wu et al. reported the formation of BiOBr nanosheets using facile co-precipitation method and illustrated a remarkable rate of inactivation of the strains of *E. coli* under visible light irradiation [266]. Similarly, Jamil et al. also reported the formation of Bismuth Oxyiodide using a facile hydrothermal technique and exhibited improved microbial inactivation results. The composites were prepared with two distinct types of solvent (ethylene glycol and distilled water) which resulted in different morphologies and also differed in the effective surface area of the composite. The inactivation results of the samples prepared with ethylene glycol showed enhanced inactivation results (complete inactivation within 45 min of irradiation) compared to the Bismuth samples prepared in distilled water [267]. Long et al. fabricated a hierarchical structure of Bismuth Oxyiodide using a facile co-precipitation method and studied the bactericidal nature of the material against the strains of *B. subtilis* and *Pseudoalteromonas*. The hierarchical property of the structure contributed to the increased surface area and also delayed the recombination rate which helped in the bacterial inactivation of up to 2-log of inactivation under 60 min of irradiation [268]. Liang et al. reported the formation of Ti-doped BiOI microspheres using the one-pot solvothermal method and studied the inactivation of *E. coli and S. aureus* under visible light irradiation. The titania loading determined the formation of the microspheres, an optimum doping amount results in the hierarchical structure which

enhances the rate of disinfection by widening the composite bandgap. Whilst, increasing the TiO$_2$ doping amount results in the deposition of amorphous titania and this restricts the growth of microspheres [269]. In a more recent study, 3D hierarchical microsphere of BiOI/BiOBr was prepared by a facile hydrothermal technique and the resulted composite exhibited improved bactericidal nature compared to bare BiOI and BiOBr under visible light irradiation. The formation of effective heterostructure contributed to the effective charge separation that necessarily sufficed the improved bactericidal behaviour of the composite [270]. Bismuth vanadate is a potential photocatalytic material but however, the poor visible light absorption is a crucial factor which needs to be addressed [271]. It exists in two crystal form; monoclinic and tetragonal. The monoclinic structure has a comparatively low band gap of 2.4 eV, while the tetragonal samples have a wide band gap of 2.9 eV [272]. Wang et al. fabricated Bismuth vanadate nanotubes and investigated the bactericidal property of the strains of *E. coli*. The nanotubes exhibited remarkable inactivation and the holes were found to be the major ROS in the inactivation process [273]. BiOI/BiVO$_4$ p–n heterojunction composite was fabricated by Xiang et al. using a facile co-precipitation method and studied the inactivation of *P. aeruginosa* under visible light irradiation. 30% BiOI/BiVO$_4$ samples were found to be the optimum doping composite efficient for the inactivation process. The scavenger experiments helped to identify the hydroxyl radicals and the holes as the potential ROS in the disinfection mechanism [274]. Adan et al. studied the bacterial inactivation efficiency of different samples of BiVO$_4$ with different doping amounts of Er^{3+} and Y^{3+}. All the bismuth samples showed a 3-log inactivation under UV and visible light irradiation. However, the metal doped composites showed improved results compared to commercial TiO$_2$ samples [275]. Booshehri et al. studied the disinfection of *E. coli, E. faecalis* and spores of *F. solani* using Ag modified Bismuth vanadate upon sunlight irradiation. The authors studied the inactivation of the composites at different silver loadings. 15 wt.% Ag composites were found to be the optimum

candidate. Moreover, the evaluation of these composites for secondary effluent from the wastewater treatment plant was performed. The results were found to be effective at a catalyst dosage of 1 g/L for all the microorganisms, solar reactors *etc*. The study also comments on the influence of the presence of inorganic and organic ions in the effluent. It was observed that the inactivation was not affected in the presence of carbonate and bicarbonate ions but the rate decelerated in the presence of organic ions. As discussed earlier, the presence of organic ions increases the competition for ROS with the microbial targets [24]. In another study, Huang et al. studied the bacterial disinfection using $BiVO_4$ and a combination of $Ag^+/BiVO_4$. The viability of the bacterial cells was observed to be unaltered when exposed to $BiVO_4$ under visible light irradiation. However, the $Ag^+/BiVO_4$ samples caused disinfection > 99% within 15 min of irradiation (Fig. 16). This indicated that the disinfection was achieved only due to the Ag ions and not due to the photocatalytic mechanism of the composite [276].

Apart from these composites, there are several other reports of novel composites of Bismuth [277–279].

7.4. Novel composites

2D nanomaterials is a fresh domain of interest within the gaggle of researchers. The investigations on graphene and its composite for disinfection studies appears to be very promising. Graphene, the favourite among the 2D class of materials has been explored to its utmost [280]. Graphene has zero potential band gaps and so the use of this material craftily has led to the formation of composites with improved photocatalytic activities. Xia et al. studied the bacterial inactivation mechanisms by graphene sheets grafted with plasmonic Ag/AgX (X = Cl, Br, I) composite under visible light irradiation. The composite prepared demonstrated an improved inactivation rate and the bacteriostatic property was attributed to the formation of ROS such as H_2O_2 in the disinfection mixture and to the bactericidal property of the Ag ions. The graphene sheets delayed the recombination rate by providing necessary charge separation [281]. In a recent study, Khadgi et al. reported the formation of $ZnFe_2O_4$ co-modified with Ag and rGO. The *E. coli* strains of bacteria were inactivated within 60 min of visible light irradiation and it showed an efficiency of more than 7-log. The SEM images of the

destructed bacterial remains are illustrated in Fig. 17. The scavenging experiments determined H_2O_2 as the main ROS species channelling the inactivation process [282].

More recently Liu et al. demonstrated the use of vertically aligned 2D MoS_2 thin films for light induced water disinfection process. The band gap of the layered MoS_2 sheets was increased but it helped in the formation of potential ROS. The bacterial inactivation was enhanced many folds compared to bulk MoS_2. The authors claimed to improve the disinfection rate by incorporating Cu film, which increased the charge separation within the layered structure and enhanced the rate of ROS production [283]. Similarly, Rtimi et al. demonstrated visibly active transparent thin films of Fe– phosphate polyethylene for bacterial inactivation. The authors found that the transparent thin film turned superhydrophilic under sunlight irradiation, which subsequently decreased the time duration for complete bacterial mineralisation from 60 to 30 min [284].

8. Commercial applications of antimicrobial photocatalysts

The rise in semiconductor photochemistry industries in the past decade is an unimpeded phenomenon after the pioneering work done by Honda and Fujishima [285]. The water splitting reaction eventually resulted in an exponential growth in green energy research for hydrogen production [286,287]. Studies exploring the use of photocatalysts led to the understanding of the light induced antibacterial phenomenon and photosterilisation. The commercial use of semiconductor photocatalyst initiated from the use of titania thin films as potential super hydrophilicity property. The thin film upon UV light irradiation generates charge carriers. These photogenerated carriers have the ability to recombine or participate in the chemical reaction on the surface. The electrons created causes reduction of the Ti^{4+} to Ti^{3+} species and a simultaneous oxidation of O^{2-} to O_2 is initiated by the photogenerated holes. This oxidation process creates oxygen vacancies, which are the site of attraction for the hydroxyl radicals. The increase in the formation of the oxygen vacancies enhances the potential to attract O_2 which effectively contribute to the hydrophilic nature. The schematic illustration of the photoinduced hydrophilicity is given in Fig. 18 [288,289].
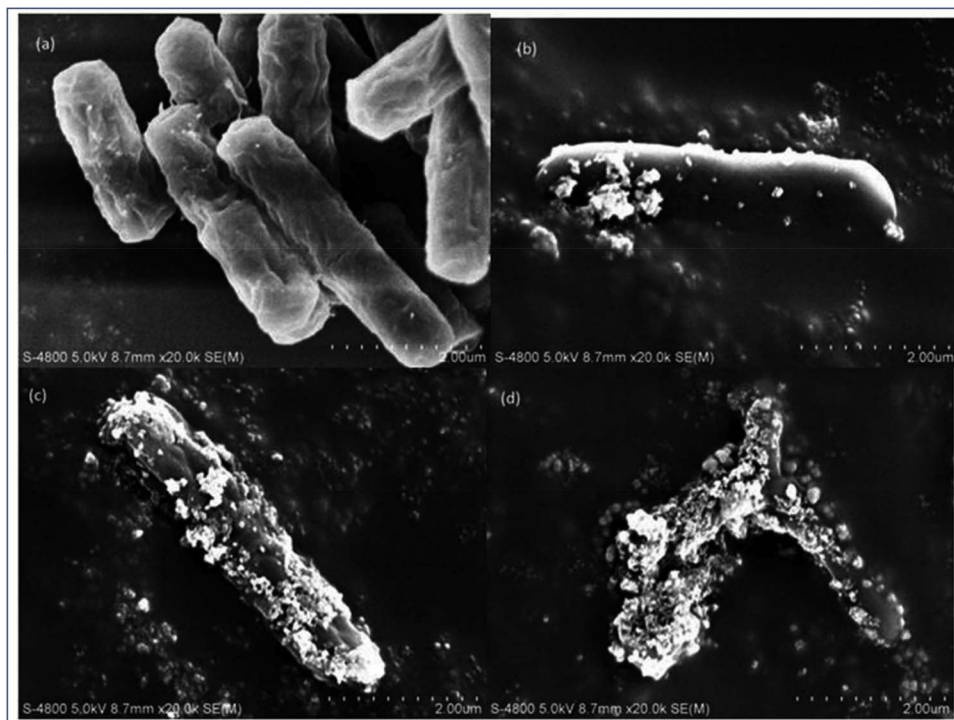

Fig. 17. SEM images of *E. coli* (a) before the addition of the nanocomposite, at the time (b) 0 min, (c) 30 min, and (d) 60 min. Reprinted with permission of Khadgi et al. Full details are given in the respective publication [282].
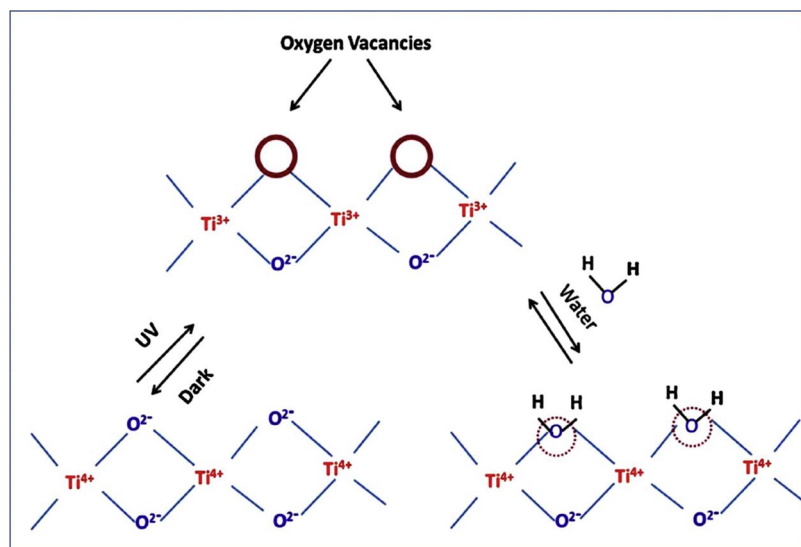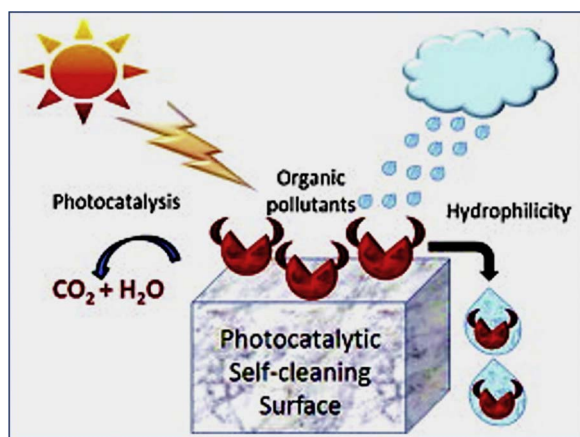
Fig. 19. Schematic illustration of the photocatalytic self-cleaning activity performed on coatings. Reprinted with permission of Banerjee et al. Full details are given in the respective publication [288].

However, the hydrophilicity behaviour is only evident under light irradiation. Although in a later study, the addition of silica or silica-based compounds enhanced the hydrophilicity even in the dark [290,291]. This property has caused its commercialisation of titania thin film coatings for self-cleaning antibacterial and antifogging applications (Fig. 19).

These coatings are widely used in several commercial products for example kitchen tiles, roof tiles, window shades *etc.*[292] Apart from titania coatings as potential self-sanitising and self-cleaning property, there exist several commercial products using metal dopants like Cu and Ag to improve the existing efficiency. The use of these typical coatings serves a multipurpose activity they preserve the aesthetic attribute of the roof tiles or any other external products and furthermore increase the durability of the product [293]. The Table 3 lists few of the industrial ventures and products available in the market utilising antimicrobial photocatalytic material for a wide range of applications.

Apart from titania, an inventory of silver based photocatalytic antimicrobial products are also widely reported [292]. The wide use of these photocatalytic materials in different applications explains the rise in this industry. Therefore, rationale design of photocatalytic materials could finally help in serving multipurpose applications out from a specific product.

9. Recommended testing methods

The rise in the use and production of antibacterial commercial products in market is self-evident, which has necessarily persuaded researchers to set clear global testing models [302]. Presently, there does not exist a standard method to determine the efficacy of these products. However, several industrial standards as outlined by ISO, ASTM and JIS which are used vividly to measure the competence of the fabricated product. Predefined standards help industries to meet the requirements of the customers and enable them to validate the effectiveness of the designed technique.

9.1. ISO standards

Different ISO standards that have widely been used for quality assurance testing include;

1. **ISO 27 447: 2009**, 'Test method for antibacterial activity of semiconducting photocatalytic materials'
2. **ISO 27 448: 2009**, 'Test method for self-cleaning performance of semiconductor photocatalytic materials − measurement of water contact angle'
3. **ISO 10 678: 2010**, 'Determination of photocatalytic activity of surfaces in an aqueous medium by degradation of methylene blue'
4. **ISO 10 676: 2010**, 'Test method for water purification performance of semiconductor photocatalytic materials by measurement of forming ability of active oxygen'
5. **ISO 10 677: 2011**, 'Ultraviolet light source for testing semiconducting photocatalytic materials'

All the above-mentioned testing standards have their own scopes as well as limitations. The present section shall discuss the ISO 27447: 2009'Test method for antibacterial activity of semiconducting photocatalytic materials' in detail.

This ISO is the standard testing technique to evaluate the antibacterial activity of photocatalytic materials as surface coatings. However, this methodology does not include any powder, granules or porous materials. Hence the present ISO technique is based on the disinfection of surface based thin film photocatalytic coatings and does not account the disinfection of air and water. In this method, there exist 2 prime routes of analysis (1) The glass adhesion method (2) The film adhesion method [288,303].

Table 3
Industrial ventures and products utilising antimicrobial photocatalytic material.

Company Details	Product name	Product description	Reference
TIPE Technologies Incorporation	VLD antibacterial photocatalytic coatings	Disinfection ability of the strains of bacteria and viruses and their mutants like MRSA, H1N1 etc.	[294]
Evonik Industries	Aeroxide TiO$_2$	Used in photocatalytic concretes, urban pavements, roof tiles etc.	[295]
Taiyo Kogyo Corporation	NEDO modified material	Membrane with antiviral and antibacterial response to indoor lighting	[296]
Green Earth nanoscience Incorporation	TiO$_2$ coating	Coatings with the self-cleaning and self-sanitising property.	[297]
Nano Land Global	Nano Photocatalyst coating	A titania self-sanitising and self-cleaning coatings	[298]
Agrob Buchtal	HT coating for ceramic tiles	Antimicrobial titania based composite coating	[299]
NanoMagic	MAGIC IQ COAT +	A TiO$_2$ based coating applied over a wide range of surface such as plastic, ceramic, fabric etc. The coating renders protection, against odour, microbes etc.	[300]
KASTUS Technologies	KASTUS glass and ceramics	Invisible, adherent TiO$_2$ coating which inactivates microbes under indoor light irradiation.	[301]

9.1.1. Glass adhesion method

This analysis method is recommended for the assessment of the antibacterial properties of fibre materials. The bacterial strains used for this assessment are *S. aureus* and *K. pneumonia*. A stock of parent strain is incubated and utilised within a week (Inoculation A). 20 mL of nutrient broth is prepared by the strains from inoculation A and further transferred to a 100 mL erlenmeyer flask. The resulted solution is agitated for 18–24 h at 110 rpm min^{-1} with an amplitude of 3 cm (Inoculation B). At the end, 0.4 mL of the inoculate B is utilised to form a 20 mL nutrient broth in a 100 mL Erlenmeyer flask, which is later incubated with agitation (Inoculation C). A 1/20'th dilution of inoculation C is utilised for the testing purpose. The cell density of the final testing aliquot is of 10^5 cells/mL. Moreover, a 50 × 50 mm test piece sample of 10 mm thickness is also prepared. Nine uncoated and 6 coated samples with photocatalysts are used for the tests [303].

The photocatalytic fabric material does not require any pre-treatment. The sample for evaluation is autoclaved initially and then inoculated with 0.2 mL of bacterial suspension as prepared as mentioned earlier using a sterile pipette. Subsequently, the test sample is placed inside the test chamber (Fig. 20) and covered with a glass to control the required levels of moisture inside the chamber. An adhesive glass of transparency greater than 85% for UV is suspended over a U-shaped glass rod placed over the filter paper. Furthermore, the sample is irradiated with a black light blue (BLB) fluorescent lamp and the intensity of the incoming irradiation is altered using perforated metal sheets. The antibacterial efficiency of the test samples is calculated utilising an antibacterial activity value [R$_L$]. The R$_L$ value is optimised by counting the presence of viable bacterial cells post illumination period (8 h) over the photocatalytic samples (C$_L$) and the non-photocatalytic samples (B$_L$). Hence R$_L$ value is calculated as: [303]

$$R_L = log\frac{B_L}{C_L} \tag{44}$$

In addition, the viable cells present over the photocatalytic samples (C$_D$) and non-photocatalytic samples (B$_D$) under dark exposure after 8 h are measured. The overall photocatalytic antibacterial activity is calculated as [303]

$$\Delta R = log\frac{B_L}{C_L} - log\frac{B_D}{C_D} \tag{45}$$

The use of the glass adhesion method for antimicrobial efficiency testing has been reported in the past literature [305]. Sadowski et al. studied the bactericidal property of titania films on organic polymers. The antimicrobial efficiency of the coating was validated by using the glass adhesion test and on irradiation of visible light [306].

9.1.2. Film adhesion method

This assessment criteria is recommended for flat surface material with photocatalytic coatings. The bacterial strains used in this assessment are *S. aureus* and *E. coli*. In this method, a stock of parent strain is inoculated in a nutrient agar culture medium and incubated for 16–24 h at 37 °C. The resulted inoculation is utilised to prepare test samples after dilution to obtain a cell count of 10^5 cells/mL. In this technique, the same experimental steps are followed as the glass adhesion method and the antibacterial efficiency is also calculated in a similar method. The assessment procedure is briefly explained in Fig. 21. The sample used in this case is a TiO$_2$/cordierite foam [303,307].

There are several reported studies utilising this standard technique to evaluate the antibacterial efficiency of the fabricated material [308–310]. Ishiguro et al. studied the microbial inactivation efficiency of TiO$_2$ coated glass over Qβ andT4 bacteriophages, using the film adhesion technique. The disarray of the protein layers is the plausible reason for viral inactivation rather the degradation of the viral RNA
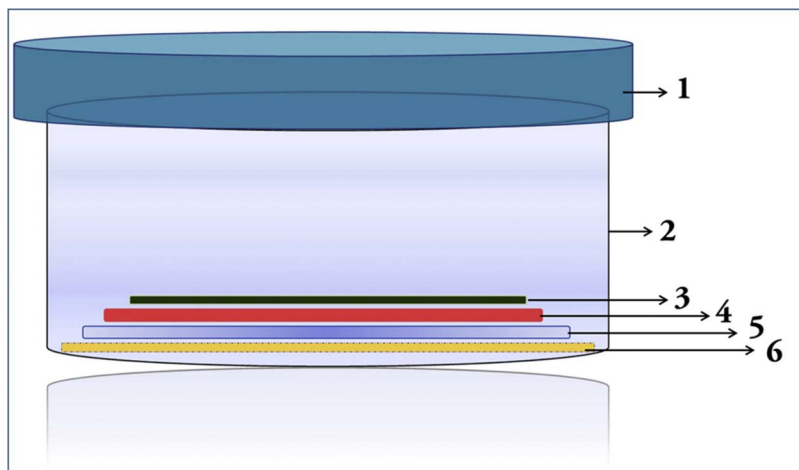
Fig. 20. Experimental setup for anti-microbial testing (1) lid, (2) petri dish, (3) adhesive film, (4) test samples with inoculated bacteria (5) U-shaped glass rod or tube and (6) moist filter paper [304].
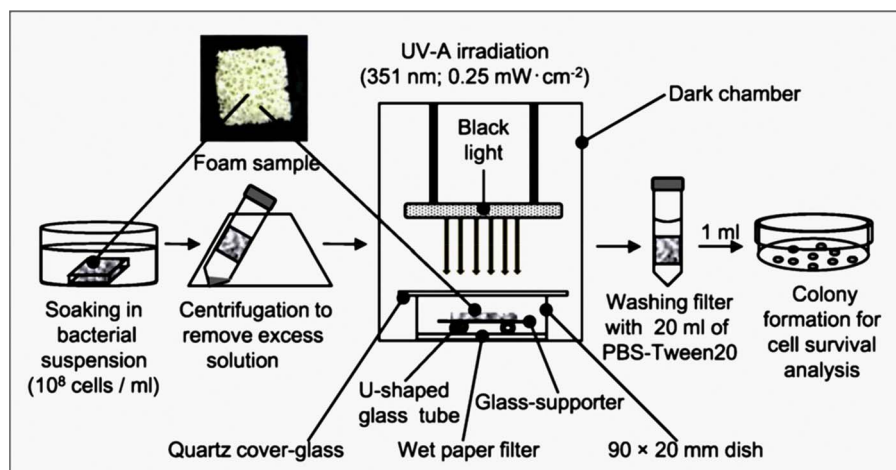
[311]. Krysa et al. conducted an assessment of the antibacterial efficiency experiments of TiO$_2$ thin films and discussed the relevance of all the conditions of the ISO standards. The authors calibrated the standards based on their laboratory conditions and additionally suggested modifications to the existing protocols. Modifications included the usage of gelatinous pills (calcium citrate + vitamins) of bacteria, and replacing the nutrient broth with saline solution. Moreover, they also suggested the use of selective media for bacteria suspension preparation [312]. Viral disinfection was also studied by using titania nanoparticles on immobilised glass plates. The authors also suggested the change in the concentration of the bovine serum in the existing ISO procedure for the viral inactivation process [313]. In a similar attempt, Ando et al. evaluated the antimicrobial efficacy of a biodegradable polymer/titania composite using a modified ISO protocols [314]. Tallosy et al. studied the bactericidal activity of titania and Ag-doped titania coatings using the ISO standard protocols under visible light irradiation and the coatings exhibited improved disinfection ability [315]. In a more recent study, Leyland et al. studied the bactericidal effect of TiO$_2$ coatings doped with Cu and F against the disinfection of strains of *S. aureus* (ATCC 6538). The coatings fabricated illustrated more than 4 log reduction under visible light irradiation (Fig. 22) [304]. In another study, Samu et al. fabricated nanoparticles of TiO$_2$ and ZnO using a template

method and further evaluated the antibacterial property of the nanomaterials using the ISO standards [316].

Despite its usefulness, however, this standard suffers from some limitations. The reported protocol does not work over rough and permeable surfaces and requires the use of two different tests for a flat surface and for fabrics. The use of two different strains for the analysis is also not justified in the process [288,303].

9.2. Japanese industrial standard (JIS)

An industrial standard, guidelines developed by a conglomerate of researchers, universities and manufacturers to evaluate the quantitative efficiency of the antimicrobial products available in the market [317]. The different antimicrobial standards under this domain are [318]:

1. **JIS L 1902:** a testing standard to evaluate the antimicrobial efficacy of the textile products. The JIS L 1902 provides a qualitative analysis of the test product using techniques known as 'halo method' "and provides quantitative estimation using two different tests known as the 'Absorption method'" "Printing method" [319–321].
2. **JIS Z 2801 2000:** a testing standard to evaluate the antimicrobial efficacy of all other products except textiles (plastics, metal, ceramic
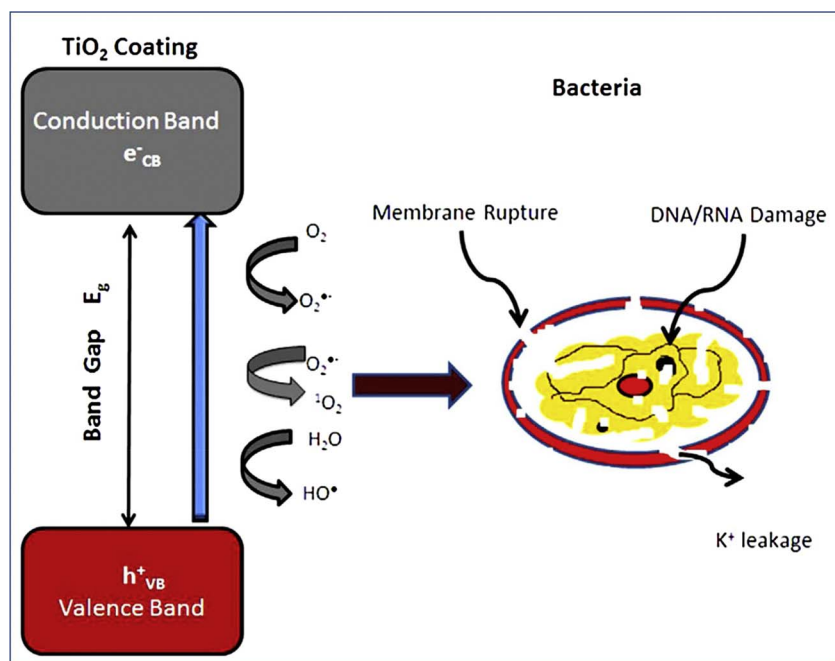

Fig. 22. Schematic representation of the photocatalytic antibacterial action. Reprinted with permission of Leyland et al. Full details are given in the respective publication [304].

etc.) [317,322,323].

3. **JIS R 1702 2012:** it is a testing standard exclusively evaluates the photocatalytic antimicrobial efficiency of the products. The present standard technique access the antibacterial potential of the products containing photocatalysts and further studies the bactericidal feature of these material under UV light irradiation (300–380 nm) [319]. The different type of tests under this standard is classified according to the shape, use and the properties of the developed product. However, the 2 definite techniques used are (a) Film adhesion technique (b) Glass adhesion method, which are similar to the ISO standards [319,324].

9.3. CEN and ASTM standards

The European Committee for standardisation has published various standards to measure the efficacy of the photocatalysts for several applications.

1. **CEN/TS 16980-1:2016 (WI = 00386023):** A standard protocol for measuring the photocatalytic degradation of nitric oxide in the air.
2. **EN 16845-1:2017 (WI = 00386022):** Procedures defined to measure the adsorbed organics and dyes on porous surface.
3. **EN 16846-1:2017 (WI = 00386018):** standard estimation protocols for photocatalytic elimination of volatile organic compounds and odour from the indoor air.
4. **prEN 17120 (WI = 00386020):** Photocatalytic water purification protocols by measuring the phenol degradation.

However, definite protocols for photocatalytic antimicrobial materials are yet to be drafted by the organisation. Presently, the European industries and researchers use the ISO standards to assess the efficacy of the developed product.

The American Section of the International Association (ASTM) is the oldest conglomerate to develop standards to evaluate the efficiency of the fabricated products available for commercial applications. Similar to the CEN standards, there does not exist any defined protocols for photocatalytic antimicrobial products in this standard.

10. Conclusions and outlook

The present review is an effort to present a comprehensive outlook of the photocatalytic antimicrobial disinfection mechanism and kinetics. In retrospect, despite the existence of several studies, the search for facile, inexpensive and visible active photocatalysts is still on going. The prevailing photocatalysts have their own limitation and the inflated cost of production with cumbersome synthetic protocols appears to be the challenge in the scaling up process for a commercial purpose. Apart from the synthesis based challenges, the rise of antibiotic resistant strains of mutant microbes is also a matter of concern. Thus far independent investigations of disinfection and inactivation of wide range of microbes has been studied extensively. Similarly, individual studies on the kinetic modelling of such inactivation process have also been carried out. However, eventually the conventional theoretical kinetic constants do not make relevance to real waste water treatment. The operational parameters and the factors affecting such processes are complex and require a concerted approach. Disinfection studies incorporating modelling data and their real waste water treatment results would aid in the process of complete understanding of the disinfection process. Amidst of all these apprehensions, photocatalytic solar disinfection is certainly an effective route for disinfection applications. The use of visible-light-induced photocatalysts for antimicrobial studies shows a promising feature to be worth exploited for commercial applications.

References

[1] M.A. Shannon, P.W. Bohn, M. Elimelech, J.G. Georgiadis, B.J. Mariñas, A.M. Mayes, Science and technology for water purification in the coming decades, Nature 452 (2008) 301–310.

[2] P.H. Gleick, The human right to water, Water policy 1 (1998) 487–503.

[3] M. Peter-Varbanets, C. Zurbrügg, C. Swartz, W. Pronk, Decentralized systems for potable water and the potential of membrane technology, Water Res. 43 (2009) 245–265.

[4] A.A. Bordalo, J. Savva-Bordalo, The quest for safe drinking water: an example from Guinea-Bissau (West Africa), Water Res. 41 (2007) 2978–2986.

[5] WH Organization, Meeting the MDG Drinking Water and Sanitation Target: the Urban and Rural Challenge of the Decade, (2006).

[6] E.J. Septimus, M.L. Schweizer, Decolonization in prevention of health care-associated infections, Clin. Microbiol. Rev. 29 (2016) 201–222.

[7] T.C. Horan, M. Andrus, M.A. Dudeck, CDC/NHSN surveillance definition of health care–associated infection and criteria for specific types of infections in the acute care setting, Am. J. Infect. Control 36 (2008) 309–332.

[8] M. Rupnik, M.H. Wilcox, D.N. Gerding, Clostridium difficile infection: new developments in epidemiology and pathogenesis, Nature reviews, Microbiology 7 (2009) 526.

[9] H.F. Chambers, F.R. DeLeo, Waves of resistance: staphylococcus aureus in the antibiotic era, Nature reviews, Microbiology 7 (2009) 629.

[10] W.H. Organization, The Burden of Health Care-associated Infection Worldwide, (2013) www wholint/gpsc/country_work/burden/hcai/en, 2013 (Last acessed on 6/10/2017).

[11] R.M. Klevens, J.R. Edwards, C.L. Richards Jr., T.C. Horan, R.P. Gaynes, D.A. Pollock, D.M. Cardo, Estimating health care-associated infections and deaths in US hospitals, 2002, Public Health Rep. 122 (2007) 160–166.

[12] D.M. Sievert, P. Ricks, J.R. Edwards, A. Schneider, J. Patel, A. Srinivasan, A. Kallen, B. Limbago, S. Fridkin, Antimicrobial-resistant pathogens associated with healthcare-associated infections summary of data reported to the National Healthcare Safety Network at the Centers for Disease Control and Prevention, 2009–2010, Infection Control Hosp. Epidemiol. 34 (2013) 1–14.

[13] L. McKibben, T. Horan, J.I. Tokars, G. Fowler, D.M. Cardo, M.L. Pearson, P.J. Brennan, H.I.C.P.A. Committee, Guidance on public reporting of healthcare-associated infections: recommendations of the Healthcare Infection Control Practices Advisory Committee, Am. J. Infect. Control 33 (2005) 217–226.

[14] D.S. Yokoe, L.A. Mermel, D.J. Anderson, K.M. Arias, H. Burstin, D.P. Calfee, S.E. Coffin, E.R. Dubberke, V. Fraser, D.N. Gerding, Executive summary: a compendium of strategies to prevent healthcare-associated infections in acute care hospitals, Infect. Control Hosp. Epidemiol. 29 (2008) S12–S21.

[15] B. Allegranzi, D. Pittet, Role of hand hygiene in healthcare-associated infection prevention, J. Hosp. Infect. 73 (2009) 305–315.

[16] A.J. Kallen, Y. Mu, S. Bulens, A. Reingold, S. Petit, K. Gershman, S.M. Ray, L.H. Harrison, R. Lynfield, G. Dumyati, Health care–associated invasive MRSA infections, 2005–2008, JAMA 304 (2010) 641–647.

[17] T. Matsunaga, R. Tomoda, T. Nakajima, H. Wake, Photoelectrochemical sterilization of microbial cells by semiconductor powders, FEMS Microbiol. Lett. 29 (1985) 211–214.

[18] S. Rtimi, C. Pulgarin, J. Kiwi, Recent developments in accelerated antibacterial inactivation on 2D Cu-titania surfaces under indoor visible light, Coatings 7 (2017) 20.

[19] J. Blanco-Galvez, P. Fernández-Ibáñez, S. Malato-Rodríguez, Solar photocatalytic detoxification and disinfection of water: recent overview, J. Solar Energy Eng. 129 (2007) 4–15.

[20] M.N. Chong, B. Jin, C.W. Chow, C. Saint, Recent developments in photocatalytic water treatment technology: a review, Water Res. 44 (2010) 2997–3027.

[21] C. McCullagh, J.M. Robertson, D.W. Bahnemann, P.K. Robertson, The application of TiO 2 photocatalysis for disinfection of water contaminated with pathogenic micro-organisms: a review, Res. Chem. Intermed. 33 (2007) 359–375.

[22] M. Pelaez, N.T. Nolan, S.C. Pillai, M.K. Seery, P. Falaras, A.G. Kontos, P.S.M. Dunlop, J.W.J. Hamilton, J.A. Byrne, K. O'Shea, M.H. Entezari, D.D. Dionysiou, A review on the visible light active titanium dioxide photocatalysts for environmental applications, Appl. Catal. B: Environ. 125 (2012) 331–349.

[23] M.R. Hoffmann, S.T. Martin, W. Choi, D.W. Bahnemann, Environmental applications of semiconductor photocatalysis, Chem. Rev. 95 (1995) 69–96.

[24] A.Y. Booshehri, M. Polo-Lopez, M. Castro-Alférez, P. He, R. Xu, W. Rong, S. Malato, P. Fernández-Ibáñez, Assessment of solar photocatalysis using Ag/BiVO 4 at pilot solar Compound Parabolic Collector for inactivation of pathogens in well water and secondary effluents, Catal. Today 281 (2017) 124–134.

[25] M.-H. Sun, S.-Z. Huang, L.-H. Chen, Y. Li, X.-Y. Yang, Z.-Y. Yuan, B.-L. Su, Applications of hierarchically structured porous materials from energy storage and conversion, catalysis, photocatalysis, adsorption, separation, and sensing to biomedicine, Chem. Soc. Rev. 45 (2016) 3479–3563.

[26] D. Spasiano, R. Marotta, S. Malato, P. Fernandez-Ibañez, I. Di Somma, Solar photocatalysis: materials, reactors, some commercial, and pre-industrialized applications. A comprehensive approach, Appl. Catal. B: Environ. 170 (2015) 90–123.

[27] D. Ravelli, D. Dondi, M. Fagnoni, A. Albini, Photocatalysis A multi-faceted concept for green chemistry, Chem. Soc. Rev. 38 (2009) 1999–2011.

[28] L. Jiang, X. Yuan, Y. Pan, J. Liang, G. Zeng, Z. Wu, H. Wang, Doping of graphitic carbon nitride for photocatalysis: a reveiw, Appl. Catal. B: Environ. 217 (2017) 388–406.

[29] L. Wang, A. Pal, J. Isaacs, D. Bello, R. Carrier, Nanomaterial induction of oxidative stress in lung epithelial cells and macrophages, J. Nanopart. Res. 16 (2014).

[30] G. Zhang, G. Liu, L. Wang, J.T. Irvine, Inorganic perovskite photocatalysts for solar energy utilization, Chem. Soc. Rev. 45 (2016) 5951–5984.

[31] X. Li, J. Yu, M. Jaroniec, Hierarchical photocatalysts, Chem. Soc. Rev. 45 (2016) 2603–2636.

[32] T. Zhang, W. Lin, Metal–organic frameworks for artificial photosynthesis and photocatalysis, Chem. Soc. Rev. 43 (2014) 5982–5993.

[33] S. Wang, Y. Zhang, F. Dong, H. Huang, Readily attainable spongy foam photocatalyst for promising practical photocatalysis, Appl. Catal. B: Environ. 208 (2017) 75–81.

[34] E. Grabowska, Selected perovskite oxides: characterization, preparation and photocatalytic properties—a review, Appl. Catal. B: Environ. 186 (2016) 97–126.

[35] H. Dumortier, S. Lacotte, G. Pastorin, R. Marega, W. Wu, D. Bonifazi, J.-P. Briand, M. Prato, S. Muller, A. Bianco, Functionalized carbon nanotubes are non-cytotoxic and preserve the functionality of primary immune cells, Nano Lett. 6 (2006) 1522–1528.

[36] T. Lammel, P. Boisseaux, M.L. Fernandez-Cruz, J.M. Navas, Internalization and cytotoxicity of graphene oxide and carboxyl graphene nanoplatelets in the human hepatocellular carcinoma cell line Hep G2, Part Fibre Toxicol. 10 (1) (2013) 27.

[37] A. Faria, A. Moraes, P. Marcato, D. Martinez, N. Durán, A. Filho, Eco-friendly decoration of graphene oxide with biogenic silver nanoparticles: antibacterial and antibiofilm activity, J. Nanopart. Res. 16 (2) (2014) 2110.

[38] M. Teta, M.M. Rankin, S.Y. Long, G.M. Stein, J.A. Kushner, Growth and regeneration of adult β cells does not involve specialized progenitors, Dev. Cell 12 (2007) 817–826.

[39] J. Li, Y. Zhu, W. Li, X. Zhang, Y. Peng, Q. Huang, Nanodiamonds as intracellular transporters of chemotherapeutic drug, Biomaterials 31 (2010) 8410–8418.

[40] L.A.V. de Luna, A.C.M. de Moraes, S.R. Consonni, C.D. Pereira, S. Cadore, S. Giorgio, O.L. Alves, Comparative in vitro toxicity of a graphene oxide-silver nanocomposite and the pristine counterparts toward macrophages, J. Nanobiotechnol. 14 (2016) 12.

[41] M. Pelaez, N.T. Nolan, S.C. Pillai, M.K. Seery, P. Falaras, A.G. Kontos, P.S. Dunlop, J.W. Hamilton, J.A. Byrne, K. O'shea, A review on the visible light active titanium dioxide photocatalysts for environmental applications, Appl. Catal. B: Environ. 125 (2012) 331–349.

[42] H. Yue, W. Wei, Z.G. Yue, B. Wang, N.N. Luo, Y.J. Gao, The role of the lateral dimension of graphene oxide in the regulation of cellular responses, Biomaterials 33 (16) (2012) 4013–4021.

[43] G. Kroemer, L. Galluzzi, P. Vandenabeele, J. Abrams, E. Alnemri, E. Baehrecke, M. Blagosklonny, W. El-Deiry, P. Golstein, D. Green, Classification of cell death: recommendations of the Nomenclature Committee on Cell Death 2009, Cell Death Different. 16 (2009) 3–11.

[44] E.H. Baehrecke, How death shapes life during development, Nat. Rev. Mol. Cell Biol. 3 (2002) 779–787.

[45] A.M. Alkilany, P.K. Nagaria, C.R. Hexel, T.J. Shaw, C.J. Murphy, M.D. Wyatt, Cellular uptake and cytotoxicity of gold nanorods: molecular origin of cytotoxicity and surface effects, Small 5 (2009) 701–708.

[46] J.F. Kerr, A.H. Wyllie, A.R. Currie, Apoptosis: a basic biological phenomenon with wide-ranging implications in tissue kinetics, Br. J. Cancer 26 (1972) 239.

[47] C. Garrido, G. Kroemer, Life's smile, death's grin: vital functions of apoptosis-executing proteins, Curr. Opin. Cell Biol. 16 (2004) 639–646.

[48] L. Galluzzi, N. Joza, E. Tasdemir, M. Maiuri, M. Hengartner, J. Abrams, N. Tavernarakis, J. Penninger, F. Madeo, G. Kroemer, No death without life: vital functions of apoptotic effectors, Cell Death Different. 15 (2008) 1113–1123.

[49] F. Zhao, Y. Zhao, Y. Liu, X. Chang, C. Chen, Y. Zhao, Cellular uptake, intracellular trafficking, and cytotoxicity of nanomaterials, Small 7 (2011) 1322–1337.

[50] V. Etacheri, C. Di Valentin, J. Schneider, D. Bahnemann, S.C. Pillai, Visible-light activation of TiO2 photocatalysts: advances in theory and experiments, J. Photochem. Photobiol. C: Photochem. Rev. 25 (2015) 1–29.

[51] J. Schneider, M. Matsuoka, M. Takeuchi, J. Zhang, Y. Horiuchi, M. Anpo, D.W. Bahnemann, Understanding TiO2 photocatalysis: mechanisms and materials, Chem. Rev. 114 (2014) 9919–9986.

[52] R. Abe, Recent progress on photocatalytic and photoelectrochemical water splitting under visible light irradiation, J. Photochem. Photobiol. C: Photochem. Rev. 11 (2010) 179–209.

[53] K. Maeda, K. Domen, Photocatalytic water splitting: recent progress and future challenges, J. Phys. Chem. Lett. 1 (2010) 2655–2661.

[54] A. Fujishima, X. Zhang, D.A. Tryk, TiO2 photocatalysis and related surface phenomena, Surf. Sci. Rep. 63 (2008) 515–582.

[55] A.M. Peiró, C. Colombo, G. Doyle, J. Nelson, A. Mills, J.R. Durrant, Photochemical reduction of oxygen adsorbed to nanocrystalline TiO2 films: a transient absorption and oxygen scavenging study of different TiO2 preparations, J. Phys. Chem. B 110 (2006) 23255–23263.

[56] A. Emeline, V. Ryabchuk, N. Serpone, Dogmas and misconceptions in heterogeneous photocatalysis. Some enlightened reflections, J. Phys. Chem. B 109 (2005) 18515–18521.

[57] P.V. Kamat, Photophysical, Photochemical and Photocatalytic Aspects of Metal Nanoparticles, ACS Publications, 2002.

[58] A. Fujishima, X. Zhang, Titanium dioxide photocatalysis: present situation and future approaches, C.R. Chim. 9 (2006) 750–760.

[59] P.V. Kamat, I. Bedja, S. Hotchandani, Photoinduced charge transfer between carbon and semiconductor clusters. One-electron reduction of C60 in colloidal TiO2 semiconductor suspensions, J. Phys. Chem. 98 (1994) 9137–9142.

[60] T. Yoshihara, R. Katoh, A. Furube, Y. Tamaki, M. Murai, K. Hara, S. Murata, H. Arakawa, M. Tachiya, Identification of reactive species in photoexcited nanocrystalline TiO2 films by wide-wavelength-range (400–2500 nm) transient absorption spectroscopy, J. Phys. Chem. B 108 (2004) 3817–3823.

[61] N. Serpone, D. Lawless, R. Khairutdinov, Size effects on the photophysical properties of colloidal anatase TiO2 particles: size quantization versus direct transitions in this indirect semiconductor? J. Phys. Chem. 99 (1995) 16646–16654.

[62] D. Lawless, N. Serpone, D. Meisel, Role of hydroxyl radicals and trapped holes in photocatalysis. A pulse radiolysis study, J. Phys. Chem. 95 (1991) 5166–5170.

[63] D.W. Bahnemann, M. Hilgendorff, R. Memming, Charge carrier dynamics at TiO2 particles: reactivity of free and trapped holes, J. Phys. Chem. B 101 (1997) 4265–4275.

[64] A. Furube, T. Asahi, H. Masuhara, H. Yamashita, M. Anpo, Charge carrier dynamics of standard TiO2 catalysts revealed by femtosecond diffuse reflectance spectroscopy, J. Phys. Chem. B 103 (1999) 3120–3127.

[65] D.P. Colombo, R.M. Bowman, Does interfacial charge transfer compete with charge carrier recombination? A femtosecond diffuse reflectance investigation of TiO2 nanoparticles, J. Phys. Chem. 100 (1996) 18445–18449.

[66] K. Iwata, T. Takaya, H.-O. Hamaguchi, A. Yamakata, T.-A. Ishibashi, H. Onishi, H. Kuroda, Carrier dynamics in TiO2 and Pt/TiO2 powders observed by femtosecond time-resolved near-infrared spectroscopy at a spectral region of 0. 9–1.5 μm with the direct absorption method, J. Phys. Chem. B 108 (2004) 20233–20239.

[67] A. Yamakata, T.-A. Ishibashi, K. Takeshita, H. Onishi, Time-resolved infrared absorption study of photochemical reactions over metal oxides, Top. Catal. 35 (2005) 211–216.

[68] C. Colbeau-Justin, M. Kunst, D. Huguenin, Structural influence on charge-carrier lifetimes in TiO2 powders studied by microwave absorption, J. Mater. Sci. 38 (2003) 2429–2437.

[69] S.T. Martin, H. Herrmann, W. Choi, M.R. Hoffmann, Time-resolved microwave conductivity. Part 1.—TiO2 photoreactivity and size quantization, J. Chem. Soc. Faraday Trans. 90 (1994) 3315–3322.

[70] S.T. Martin, H. Herrmann, M.R. Hoffmann, Time-resolved microwave conductivity. Part 2.—Quantum-sized TiO2 and the effect of adsorbates and light intensity on charge-carrier dynamics, J. Chem. Soc. Faraday Trans. 90 (1994) 3323–3330.

[71] A. Furube, T. Asahi, H. Masuhara, H. Yamashita, M. Anpo, Direct observation of a picosecond charge separation process in photoexcited platinum-loaded TiO2 particles by femtosecond diffuse reflectance spectroscopy, Chem. Phys. Lett. 336 (2001) 424–430.

[72] A. Henglein, Small-particle research: physicochemical properties of extremely small colloidal metal and semiconductor particles, Chem. Rev. 89 (1989) 1861–1873.

[73] U. Kolle, J. Moser, M. Gratzel, Dynamics of interfacial charge-transfer reactions in semiconductor dispersions. Reduction of cobaltoceniumdicarboxylate in colloidal TiO2, Inorg. Chem. 24 (1985) 2253–2258.

[74] S.H. Szczepankiewicz, A. Colussi, M.R. Hoffmann, Infrared spectra of photoinduced species on hydroxylated titania surfaces, J. Phys. Chem. B 104 (2000) 9842–9850.

[75] D. Bahnemann, A. Henglein, J. Lilie, L. Spanhel, Flash photolysis observation of the absorption spectra of trapped positive holes and electrons in colloidal titanium dioxide, J. Phys. Chem. 88 (1984) 709–711.

[76] S.T. Martin, C.L. Morrison, M.R. Hoffmann, Photochemical mechanism of size-quantized vanadium-doped TiO2 particles, J. Phys. Chem. 98 (1994) 13695–13704.

[77] X. Yang, N. Tamai, How fast is interfacial hole transfer? In situ monitoring of carrier dynamics in anatase TiO2 nanoparticles by femtosecond laser spectroscopy, Phys. Chem. Chem. Phys. 3 (2001) 3393–3398.

[78] A. Yamakata, T.-A. Ishibashi, H. Onishi, Water-and oxygen-induced decay kinetics of photogenerated electrons in TiO2 and Pt/TiO2: a time-resolved infrared absorption study, J. Phys. Chem. B 105 (2001) 7258–7262.

[79] Y. Tamaki, A. Furube, R. Katoh, M. Murai, K. Hara, H. Arakawa, M. Tachiya, Trapping dynamics of electrons and holes in a nanocrystalline TiO2 film revealed by femtosecond visible/near-infrared transient absorption spectroscopy, C.R. Chim. 9 (2006) 268–274.

[80] Y. Tamaki, A. Furube, M. Murai, K. Hara, R. Katoh, M. Tachiya, Dynamics of efficient electron–hole separation in TiO2 nanoparticles revealed by femtosecond transient absorption spectroscopy under the weak-excitation condition, Phys. Chem. Chem. Phys. 9 (2007) 1453–1460.

[81] E. Tasdemir, L. Galluzzi, M.C. Maiuri, A. Criollo, I. Vitale, E. Hangen, N. Modjtahedi, G. Kroemer, Methods for assessing autophagy and autophagic cell death, Autophagosome Phagosome (2008) 29–76.

[82] B. Levine, G. Kroemer, Autophagy in the pathogenesis of disease, Cell 132 (2008) 27–42.

[83] R.-A. González-Polo, P. Boya, A.-L. Pauleau, A. Jalil, N. Larochette, S. Souquère, E.-L. Eskelinen, G. Pierron, P. Saftig, G. Kroemer, The apoptosis/autophagy paradox: autophagic vacuolization before apoptotic death, J. Cell Sci. 118 (2005) 3091–3102.

[84] S.R. Saptarshi, A. Duschl, A.L. Lopata, Interaction of nanoparticles with proteins:

relation to bio-reactivity of the nanoparticle, J. Nanobiotechnol. 11 (2013) 26.

[85] S. Chakravarthi, C.E. Jessop, N.J. Bulleid, The role of glutathione in disulphide bond formation and endoplasmic-reticulum-generated oxidative stress, EMBO Rep. 7 (2006) 271–275.

[86] W. Stahl, A. Junghans, B. de Boer, E.S. Driomina, K. Briviba, H. Sies, Carotenoid mixtures protect multilamellar liposomes against oxidative damage: synergistic effects of lycopene and lutein, FEBS Lett. 427 (1998) 305–308.

[87] K. Apel, H. Hirt, Reactive oxygen species: metabolism, oxidative stress, and signal transduction, Annu. Rev. Plant Biol. 55 (2004) 373–399.

[88] L. Jornot, H. Petersen, A.F. JUNOD, Hydrogen peroxide-induced DNA damage is independent of nuclear calcium but dependent on redox-active ions, Biochem. J. 335 (1998) 85–94.

[89] L. Hajba, A. Guttman, The use of magnetic nanoparticles in cancer theranostics: toward handheld diagnostic devices, Biotechnol. Adv. 34 (2016) 354–361.

[90] K. Vinodgopal, P.V. Kamat, Photochemistry on surfaces: photodegradation of 1 3-diphenylisobenzofuran over metal oxide particles, J. Phys. Chem. 96 (1992) 5053–5059.

[91] V. Mailander, K. Landfester, Interaction of nanoparticles with cells, Biomacromolecules 10 (2009) 2379–2400.

[92] W. Jiang, B.Y. Kim, J.T. Rutka, W.C. Chan, Nanoparticle-mediated cellular response is size-dependent, Nat. Nanotechnol. 3 (2008) 145–150.

[93] N. Liu, Y. Chang, Y. Feng, Y. Cheng, X. Sun, H. Jian, Y. Feng, X. Li, H. Zhang, {101}–{001} surface heterojunction-Enhanced antibacterial activity of titanium dioxide nanocrystals under sunlight irradiation, ACS Appl. Mater. Interfaces 9 (2017) 5907–5915.

[94] H.A. Foster, I.B. Ditta, S. Varghese, A. Steele, Photocatalytic disinfection using titanium dioxide: spectrum and mechanism of antimicrobial activity, Appl. Microbiol. Biotechnol. 90 (2011) 1847–1868.

[95] M.J. Abeledo-Lameiro, A. Reboredo-Fernández, M.I. Polo-López, P. Fernández-Ibáñez, E. Ares-Mazás, H. Gómez-Couso, Photocatalytic inactivation of the waterborne protozoan parasite Cryptosporidium parvum using TiO2/H2O2 under simulated and natural solar conditions, Catal. Today 280 (2017) 132–138.

[96] K.R. Kunduru, M. Nazarkovsky, S. Farah, R.P. Pawar, A. Basu, A.J. Domb, Nanotechnology for water purification: applications of nanotechnology methods In wastewater treatment, Water Purif. (2016) 33.

[97] M. Wang, Y. Ni, A. Liu, Resorcinol–Formaldehyde Resin/Cu2O composite microstructures: solution-Phase construction, magnetic performance, and applications in antibacterial and catalytic fields, ACS Omega 2 (2017) 1505–1512.

[98] B. Kim, D. Kim, D. Cho, S. Cho, Bactericidal effect of TiO2 photocatalyst on selected food-borne pathogenic bacteria, Chemosphere 52 (2003) 277–281.

[99] A.J. Macpherson, N.L. Harris, Interactions between commensal intestinal bacteria and the immune system, Nat. Rev. Immunol. 4 (2004) 478–485.

[100] H.H. Zahran, Rhizobium-legume symbiosis and nitrogen fixation under severe conditions and in an arid climate, Microbiol. Mol. Biol. Rev. 63 (1999) 968–989.

[101] C.A. Kellogg, D.W. Griffin, Aerobiology and the global transport of desert dust, Trends Ecol. Evol. 21 (2006) 638–644.

[102] P.H. Lebre, P. De Maayer, D.A. Cowan, Xerotolerant bacteria: surviving through a dry spell, Nat. Rev. Microbiol. 15 (2017) 285–296.

[103] P. Bonfante, A. Desirò, Who lives in a fungus? The diversity, origins and functions of fungal endobacteria living in Mucoromycota, ISME J. 11 (2017) 1727–1735.

[104] H.J. Wagner, C.C. Capitain, K. Richter, M. Nessling, J. Mampel, Engineering bacterial microcompartments with heterologous enzyme cargos, Eng. Life Sci. 17 (2017) 36–46.

[105] J.A. Fuerst, Intracellular compartmentation in planctomycetes, Annu. Rev. Microbiol. 59 (2005) 299–328.

[106] M.R. Lindsay, R.I. Webb, M. Strous, M.S. Jetten, M.K. Butler, R.J. Forde, J.A. Fuerst, Cell compartmentalisation in planctomycetes: novel types of structural organisation for the bacterial cell, Arch. Microbiol. 175 (2001) 413–429.

[107] C. Robinow, E. Kellenberger, The bacterial nucleoid revisited, Microbiol. Rev. 58 (1994) 211–232.

[108] R.N. Doetsch, T.M. Cook, Introduction to bacteria and their ecobiology, Springer Sci. Business Media (2012).

[109] K.H. Schleifer, O. Kandler, Peptidoglycan types of bacterial cell walls and their taxonomic implications, Bacteriol. Rev. 36 (1972) 407.

[110] W.W. Navarre, O. Schneewind, Surface proteins of gram-positive bacteria and mechanisms of their targeting to the cell wall envelope, Microbiol. Mol. Biol. Rev. 63 (1999) 174–229.

[111] J.R. Tagg, A.S. Dajani, L.W. Wannamaker, Bacteriocins of gram-positive bacteria, Bacteriol. Rev. 40 (1976) 722.

[112] S. Halebian, B. Harris, S. Finegold, R. Rolfe, Rapid method that aids in distinguishing Gram-positive from Gram-negative anaerobic bacteria, J. Clin. Microbiol. 13 (1981) 444–448.

[113] L. Brown, J.M. Wolf, R. Prados-Rosales, A. Casadevall, Through the wall: extracellular vesicles in Gram-positive bacteria, mycobacteria and fungi, Nat. Rev. Microbiol. 13 (2015) 620–630.

[114] A. Schatz, E. Bugie, S.A. Waksman, Streptomycin, a substance exhibiting antibiotic activity against gram-Positive and gram-Negative bacteria.∗, Proc. Soc. Exp. Biol. Med. 55 (1944) 66–69.

[115] J.A. Fuerst, Beyond prokaryotes and eukaryotes: planctomycetes and cell organization, Nat. Educ 3 (2010) 44.

[116] M. van der Giezen, J. Tovar, C.G. Clark, Mitochondrion-Derived organelles in protists and fungi, Int. Rev. Cytol. 244 (2005) 175–225.

[117] S. Bartnicki-Garcia, Cell chemistry, morphogenesis, and taxonomy of fungi, Annu. Rev. Microbiol. 22 (1968) 87–108.

[118] R.A. Muzzarelli, Chitin, Elsevier, 2013.

[119] L.G. Sancho, R. De la Torre, G. Horneck, C. Ascaso, A. de los Rios, A. Pintado,

[120] J. Wierzchos, M. Schuster, Lichens survive in space: results from the 2005 LICHENS experiment, Astrobiology 7 (2007) 443–454.

[121] L. Burgess, General ecology of the Fusaria, Fusarium: diseases, Biol. Taxonomy (1981) 225–235.

[122] S. Ruisi, D. Barreca, L. Selbmann, L. Zucconi, S. Onofri, Fungi in Antarctica, Rev. Environ. Sci. Bio/Technol. 6 (2007) 127–141.

[123] S.E. Hardison, G.D. Brown, C-type lectin receptors orchestrate antifungal immunity, Nat. Immunol. 13 (2012) 817–822.

[124] D. Wessner, The origins of viruses, Nat. Edu. 3 (2010) 37.

[125] E.C. Holmes, The Evolution and Emergence of RNA Viruses, Oxford University Press, 2009.

[126] S. Sierra, B. Kupfer, R. Kaiser, Basics of the virology of HIV-1 and its replication, J. Clin. Virol. 34 (2005) 233–244.

[127] D.S. Goodsell, A.J. Olson, Structural symmetry and protein function, Annu. Rev. Biophys. Biomol. Struct. 29 (2000) 105–153.

[128] P. Ceres, A. Zlotnick, Weak protein- protein interactions are sufficient to drive assembly of hepatitis B virus capsids, Biochemistry 41 (2002) 11525–11531.

[129] M. Roivainen, L. Piirainen, T. Hovi, I. Virtanen, T. Riikonen, J. Heino, T. Hyypiä, Entry of coxsackievirus A9 into host cells: specific interactions with αvβ3 integrin, the vitronectin receptor, Virology 203 (1994) 357–365.

[130] H.L. Ploegh, Viral strategies of immune evasion, Science 280 (1998) 248–253.

[131] X. Wang, L. Zhu, M. Dang, Z. Hu, Q. Gao, S. Yuan, Y. Sun, B. Zhang, J. Ren, A. Kotecha, Potent neutralization of hepatitis A virus reveals a receptor mimic mechanism and the receptor recognition site, Proc. Natl. Acad. Sci. (2017) 201616502.

[132] S. Sharma, S. Chatterjee, S. Datta, R. Prasad, D. Dubey, R.K. Prasad, M.G. Vairale, Bacteriophages and its applications: an overview, Folia Microbiol. (Praha) 62 (2017) 17–55.

[133] S. Tripathi, V.R. Balasubramaniam, J.A. Brown, I. Mena, A. Grant, S.V. Bardina, K. Maringer, M.C. Schwarz, A.M. Maestre, M. Sourisseau, A novel Zika virus mouse model reveals strain specific differences in virus pathogenesis and host inflammatory immune responses, PLoS Pathog. 13 (3) (2017) e1006258.

[134] H.C. Bold, M. Wynne, Introduction to the algae: structure and reproduction, Prentice Hall (1978).

[135] M.M. Allen, Simple conditions for growth of unicellular blue-green algae on plates, J. Phycol. 4 (1968) 1–4.

[136] D. Fawcett, J.J. Verduin, M. Shah, S.B. Sharma, G.E.J. Poinern, A review of current research into the biogenic synthesis of metal and metal oxide nanoparticles via marine algae and seagrasses, Journal of Nanoscience 2017 (2017) 8013850.

[137] P. Ditsche, M. Hicks, L. Truong, C. Linkem, A. Summers, From smooth to rough, from water to air: the intertidal habitat of Northern clingfish (Gobiesox maeandricus), Sci. Nat. 104 (2017) 33.

[138] É.C. Schmidt, L.A. Scariot, T. Rover, Z.L. Bouzon, Changes in ultrastructure and histochemistry of two red macroalgae strains of Kappaphycus alvarezii (Rhodophyta Gigartinales), as a consequence of ultraviolet B radiation exposure, Micron 40 (2009) 860–869.

[139] P. Albersheim, A. Darvill, K. Roberts, R. Sederoff, A. Staehelin, Plant cell walls, Garland Sci. (2010).

[140] L.A. Lewis, R.M. McCourt, Green algae and the origin of land plants, Am. J. Bot. 91 (2004) 1535–1556.

[141] M. Ohtani, N. Akiyoshi, Y. Takenaka, R. Sano, T. Demura, Evolution of plant conducting cells: perspectives from key regulators of vascular cell differentiation, J. Exp. Bot. 68 (2017) 17–26.

[142] J. Meriluoto, L. Blaha, G. Bojadzija, M. Bormans, L. Brient, G.A. Codd, D. Drobac, E.J. Faassen, J. Fastner, A. Hiskia, Toxic cyanobacteria and cyanotoxins in European waters–recent progress achieved through the CYANOCOST Action and challenges for further research, Adv. Oceanogr. Limnol. 8 (2017).

[143] E. Dittmann, C. Wiegand, Cyanobacterial toxins–occurrence, biosynthesis and impact on human affairs, Mol. Nutr. Food Res. 50 (2006) 7–17.

[144] S.D. Richardson, S.Y. Kimura, Emerging environmental contaminants: challenges facing our next generation and potential engineering solutions, Environ. Technol. Innov. (2017).

[145] H. Xu, H. Pei, Y. Jin, H. Xiao, C. Ma, J. Sun, H. Li, Characteristics of water obtained by dewatering cyanobacteria-containing sludge formed during drinking water treatment, including C- N-disinfection byproduct formation, Water Res. 111 (2017) 382–392.

[146] B.C. Hitzfeld, S.J. Höger, D.R. Dietrich, Cyanobacterial toxins: removal during drinking water treatment, and human risk assessment, Environ. Health Perspect. 108 (2000) 113.

[147] J.A. Ibáñez, M.I. Litter, R.A. Pizarro, Photocatalytic bactericidal effect of TiO2 on Enterobacter cloacae: comparative study with other Gram (−) bacteria, J. Photochem. Photobiol. A: Chem. 157 (2003) 81–85.

[148] Y. Li, W. Zhang, J. Niu, Y. Chen, Mechanism of photogenerated reactive oxygen species and correlation with the antibacterial properties of engineered metal-oxide nanoparticles, ACS Nano 6 (2012) 5164–5173.

[149] T. Saito, T. Iwase, J. Horie, T. Morioka, Mode of photocatalytic bactericidal action of powdered semiconductor TiO2 on mutans streptococci, J. Photochem. Photobiol. B 14 (1992) 369–379.

[150] Y. Kikuchi, K. Sunada, T. Iyoda, K. Hashimoto, A. Fujishima, Photocatalytic bactericidal effect of TiO2 thin films: dynamic view of the active oxygen species responsible for the effect, J. Photochem. Photobiol. A: Chem. 106 (1997) 51–56.

[151] W.A. Jacoby, P.C. Maness, E.J. Wolfrum, D.M. Blake, J.A. Fennell, Mineralization of bacterial cell mass on a photocatalytic surface in air, Environ. Sci. Technol. 32 (1998) 2650–2653.

[152] P.-C. Maness, S. Smolinski, D.M. Blake, Z. Huang, E.J. Wolfrum, W.A. Jacoby, Bactericidal activity of photocatalytic TiO2 reaction: toward an understanding of

its killing mechanism, Appl. Environ. Microbiol. 65 (1999) 4094–4098.

[152] D. Bagchi, M. Bagchi, E. Hassoun, S. Stohs, Detection of paraquat-induced in vivo lipid peroxidation by gas chromatography/mass spectrometry and high-pressure liquid chromatography, J. Anal. Toxicol. 17 (1993) 411–414.

[153] M. Sökmen, F. Candan, Z. Sümer, Disinfection of E. coli by the Ag-TiO2/UV system: lipidperoxidation, J. Photochem. Photobiol. A: Chem. 143 (2001) 241–244.

[154] J. Kiwi, V. Nadtochenko, Evidence for the mechanism of photocatalytic degradation of the bacterial wall membrane at the TiO2 interface by ATR-FTIR and laser kinetic spectroscopy, Langmuir 21 (2005) 4631–4641.

[155] S. Pigeot-Rémy, F. Simonet, E. Errazuriz-Cerda, J. Lazzaroni, D. Atlan, C. Guillard, Photocatalysis and disinfection of water: identification of potential bacterial targets, Appl. Catal. B: Environ. 104 (2011) 390–398.

[156] W. Wang, L. Zhang, T. An, G. Li, H.-Y. Yip, P.-K. Wong, Comparative study of visible-light-driven photocatalytic mechanisms of dye decolorization and bacterial disinfection by B–Ni-codoped TiO2 microspheres: the role of different reactive species, Appl. Catal. B: Environ. 108 (2011) 108–116.

[157] I. Matai, A. Sachdev, P. Dubey, S.U. Kumar, B. Bhushan, P. Gopinath, Antibacterial activity and mechanism of Ag–ZnO nanocomposite on S. aureus and GFP-expressing antibiotic resistant E. coli, Colloids Surf. B: Biointerfaces 115 (2014) 359–367.

[158] D.F. Ollis, Kinetics of liquid phase photocatalyzed reactions: an illuminating approach, J. Phys. Chem. B 109 (2005) 2439–2444.

[159] M.L. Satuf, M.J. Pierrestegui, L. Rossini, R.J. Brandi, O.M. Alfano, Kinetic modeling of azo dyes photocatalytic degradation in aqueous TiO2 suspensions. Toxicity and biodegradability evaluation, Catal. Today 161 (2011) 121–126.

[160] C. Passalía, M.E. Martínez Retamar, O.M. Alfano, R.J. Brandi, Photocatalytic degradation of formaldehyde in gas phase on TiO2 films: a kinetic study, Int. J. Chem. Reactor Eng. 8 (2010).

[161] C. Minero, F. Catozzo, E. Pelizzetti, Role of adsorption in photocatalyzed reactions of organic molecules in aqueous titania suspensions, Langmuir 8 (1992) 481–486.

[162] S.J. Thomson, G.C. Webb, Heterogeneous catalysis, Wiley (1968).

[163] J.-M. Herrmann, Photocatalysis fundamentals revisited to avoid several misconceptions, Appl. Catal. B: Environ. 99 (2010) 461–468.

[164] D. Monllor-Satoca, R. Gómez, M. González-Hidalgo, P. Salvador, The Direct–Indirect model: an alternative kinetic approach in heterogeneous photocatalysis based on the degree of interaction of dissolved pollutant species with the semiconductor surface, Catal. Today 129 (2007) 247–255.

[165] H. Gerischer, Photocatalysis in aqueous solution with small TiO2 particles and the dependence of the quantum yield on particle size and light intensity, Electrochim. Acta 40 (1995) 1277–1281.

[166] R.A. Marcus, On the theory of oxidation-reduction reactions involving electron transfer. I, J. Chem. Phys. 24 (1956) 966–978.

[167] H. Gerischer, Charge transfer processes at semiconductor-electrolyte interfaces in connection with problems of catalysis, Surf. Sci. 18 (1969) 97–122.

[168] H. Gerischer, W. Mindt, The mechanisms of the decomposition of semiconductors by electrochemical oxidation and reduction, Electrochim. Acta 13 (1968) 1329–1341.

[169] C. Minero, Kinetic analysis of photoinduced reactions at the water semiconductor interface, Catal. Today 54 (1999) 205–216.

[170] J. Montoya, J. Velasquez, P. Salvador, The direct–indirect kinetic model in photocatalysis: a reanalysis of phenol and formic acid degradation rate dependence on photon flow and concentration in TiO 2 aqueous dispersions, Appl. Catal. B: Environ. 88 (2009) 50–58.

[171] S. Valencia, F. Catano, L. Rios, G. Restrepo, J. Marín, A new kinetic model for heterogeneous photocatalysis with titanium dioxide: case of non-specific adsorption considering back reaction, Appl. Catal. B: Environ. 104 (2011) 300–304.

[172] A. Mills, C. O'Rourke, K. Moore, Powder semiconductor photocatalysis in aqueous solution: an overview of kinetics-based reaction mechanisms, J. Photochem. Photobiol. A: Chem. 310 (2015) 66–105.

[173] J. Montoya, J. Peral, P. Salvador, Commentary on the article:A new kinetic model for heterogeneous photocatalysis with titanium dioxide: case of non-specific adsorption considering back reaction, by S. Valencia, F., Catano, L., Rios, G. Restrepo and J. Marin, published in Applied Catalysis B: Environmental, 104 (2011) 300–304, Appl. Catal. B: Environ. 111 (2012) 649–650.

[174] J.F. Montoya, J. Peral, P. Salvador, Comprehensive kinetic and mechanistic analysis of TiO2 photocatalytic reactions according to the Direct–Indirect Model:(I) theoretical approach, J. Phys. Chem. C 118 (2014) 14266–14275.

[175] P. Salvador, On the nature of photogenerated radical species active in the oxidative degradation of dissolved pollutants with TiO2 aqueous suspensions: a revision in the light of the electronic structure of adsorbed water, J. Phys. Chem. C 111 (2007) 17038–17043.

[176] B.F. Severin, M.T. Suidan, R.S. Engelbrecht, Kinetic modeling of UV disinfection of water, Water Res. 17 (1983) 1669–1678.

[177] J. Moreno-Andrés, L. Romero-Martínez, A. Acevedo-Merino, E. Nebot, UV-based technologies for marine water disinfection and the application to ballast water: does salinity interfere with disinfection processes? Sci. Total Environ. 581 (2017) 144–152.

[178] D. Venieri, D. Mantzavinos, Disinfection of Waters/Wastewaters by Solar Photocatalysis, Advances in Photocatalytic Disinfection, Springer, 2017, pp. 177–198.

[179] L.L. Gyürék, G.R. Finch, Modeling water treatment chemical disinfection kinetics, J. Environ. Eng. 124 (1998) 783–793.

[180] J. Marugán, R. Van Grieken, C. Pablos, M.L. Satuf, A.E. Cassano, O.M. Alfano, Rigorous kinetic modelling with explicit radiation absorption effects of the photocatalytic inactivation of bacteria in water using suspended titanium dioxide, Appl. Catal. B: Environ. 102 (2011) 404–416.

[181] M. Cho, H. Chung, J. Yoon, Disinfection of water containing natural organic matter by using ozone-initiated radical reactions, Appl. Environ. Microbiol. 69 (2003) 2284–2291.

[182] R. Sadiq, M.J. Rodriguez, Disinfection by-products (DBPs) in drinking water and predictive models for their occurrence: a review, Sci. Total Environ. 321 (2004) 21–46.

[183] O.K. Dalrymple, E. Stefanakos, M.A. Trotz, D.Y. Goswami, A review of the mechanisms and modeling of photocatalytic disinfection, Appl. Catal. B: Environ. 98 (2010) 27–38.

[184] J.C. Hoff, Inactivation of Microbial Agents by Chemical Disinfectants, (1986).

[185] M.Y. Lim, J.-M. Kim, G. Ko, Disinfection kinetics of murine norovirus using chlorine and chlorine dioxide, Water Res. 44 (2010) 3243–3251.

[186] X. Ma, K. Bibby, Free chlorine and monochloramine inactivation kinetics of Aspergillus and Penicillium in drinking water, Water Res. (2017).

[187] H.E. Watson, A note on the variation of the rate of disinfection with change in the concentration of the disinfectant, J. Hyg. (Lond.) 8 (1908) 536–542.

[188] J. Marugán, R. van Grieken, C. Sordo, C. Cruz, Kinetics of the photocatalytic disinfection of Escherichia coli suspensions, Appl. Catal. B: Environ. 82 (2008) 27–36.

[189] M.A. Benarde, W.B. Snow, V.P. Olivieri, B. Davidson, Kinetics and mechanism of bacterial disinfection by chlorine dioxide, Appl. Microbiol. 15 (1967) 257–265.

[190] C.N. Haas, A mechanistic kinetic model for chlorine disinfection, Environ. Sci. Technol. 14 (1980) 339–340.

[191] C.N. Haas, S.B. Karra, Kinetics of microbial inactivation by chlorine—I. Review of results in demand-free systems, Water Res. 18 (1984) 1443–1449.

[192] L.L. del Carmen Huesca-Espitia, V. Aurioles-López, I. Ramírez, J.L. Sánchez-Salas, E.R. Bandala, Photocatalytic inactivation of highly resistant microorganisms in water: a kinetic approach, J. Photochem. Photobiol. A: Chem. 337 (2017) 132–139.

[193] J.L. Rennecker, B.J. Mariñas, J.H. Owens, E.W. Rice, Inactivation of Cryptosporidium parvum oocysts with ozone, Water Res. 33 (1999) 2481–2488.

[194] M. Cho, H. Chung, W. Choi, J. Yoon, Linear correlation between inactivation of E. coli and OH radical concentration in TiO2 photocatalytic disinfection, Water Res. 38 (2004) 1069–1077.

[195] M. Cho, Y. Lee, W. Choi, H. Chung, J. Yoon, Study on Fe (VI) species as a disinfectant: quantitative evaluation and modeling for inactivating Escherichia coli, Water Res. 40 (2006) 3580–3586.

[196] C.N. Haas, J. Joffe, Disinfection under dynamic conditions: modification of Hom's model for decay, Environ. Sci. Technol. 28 (1994) 1367–1369.

[197] M.N. Chong, B. Jin, C.P. Saint, Bacterial inactivation kinetics of a photo-disinfection system using novel titania-impregnated kaolinite photocatalyst, Chem. Eng. J. 171 (2011) 16–23.

[198] M. Castro-Alférez, M.I. Polo-López, J. Marugán, P. Fernández-Ibáñez, Mechanistic model of the Escherichia coli inactivation by solar disinfection based on the photogeneration of internal ROS and the photo-inactivation of enzymes: CAT and SOD, Chem. Eng. J. 318 (2017) 214–223.

[199] R.J. Watts, S. Kong, M.P. Orr, G.C. Miller, B.E. Henry, Photocatalytic inactivation of coliform bacteria and viruses in secondary wastewater effluent, Water Res. 29 (1995) 95–100.

[200] A.-G. Rincon, C. Pulgarin, Effect of pH, inorganic ions, organic matter and H2O2 on E. coli K12 photocatalytic inactivation by TiO2: implications in solar water disinfection, Appl. Catal. B: Environ. 51 (2004) 283–302.

[201] A. Rincón, C. Pulgarin, Photocatalytical inactivation of E. coli: effect of (continuous–intermittent) light intensity and of (suspended–fixed) TiO2 concentration, Appl. Catal. B: Environ. 44 (2003) 263–284.

[202] A.-G. Rincón, C. Pulgarin, Bactericidal action of illuminated TiO2 on pure Escherichia coli and natural bacterial consortia: post-irradiation events in the dark and assessment of the effective disinfection time, Appl. Catal. B: Environ. 49 (2004) 99–112.

[203] D. Gumy, A. Rincon, R. Hajdu, C. Pulgarin, Solar photocatalysis for detoxification and disinfection of water: different types of suspended and fixed TiO2 catalysts study, Sol. Energy 80 (2006) 1376–1381.

[204] A.-G. Rincón, C. Pulgarin, Field solar E. coli inactivation in the absence and presence of TiO2: is UV solar dose an appropriate parameter for standardization of water solar disinfection? Sol. Energy 77 (2004) 635–648.

[205] N. Daneshvar, D. Salari, A. Khataee, Photocatalytic degradation of azo dye acid red 14 in water on ZnO as an alternative catalyst to TiO2, J. Photochem. Photobiol. A: Chem. 162 (2004) 317–322.

[206] J.H. Melián, J.D. Rodríguez, A.V. Suárez, E.T. Rendón, C.V. Do Campo, J. Arana, J.P. Peña, The photocatalytic disinfection of urban waste waters, Chemosphere 41 (2000) 323–327.

[207] M. Murdoch, G. Waterhouse, M. Nadeem, J. Metson, M. Keane, R. Howe, J. Llorca, H. Idriss, The effect of gold loading and particle size on photocatalytic hydrogen production from ethanol over Au/TiO2 nanoparticles, Nat. Chem. 3 (2011) 489.

[208] A. Akyol, H. Yatmaz, M. Bayramoglu, Photocatalytic decolorization of remazol red RR in aqueous ZnO suspensions, Appl. Catal. B: Environ. 54 (2004) 19–24.

[209] H.C. Yatmaz, N. Dizge, M.S. Kurt, Combination of photocatalytic and membrane distillation hybrid processes for reactive dyes treatment, Environ. Technol. (2016) 1–25.

[210] D. Bahnemann, Solar photocatalytic disinfection of water, Photocatal.: Applic. 15 (2016) 72.

[211] S. Malato, M.I. Maldonado, P. Fernandez-Ibanez, I. Oller, I. Polo, R. Sanchez-Moreno, Decontamination and disinfection of water by solar photocatalysis: the pilot plants of the Plataforma Solar de Almeria, Mater. Sci. Semicond. Process. 42 (2016) 15–23.

[212] A. Benabbou, Z. Derriche, C. Felix, P. Lejeune, C. Guillard, Photocatalytic

inactivation of Escherischia coli: effect of concentration of TiO2 and micro-organism, nature, and intensity of UV irradiation, Appl. Catal. B: Environ. 76 (2007) 257–263.

[213] L. Caballero, K. Whitehead, N. Allen, J. Verran, Inactivation of Escherichia coli on immobilized TiO2 using fluorescent light, J. Photochem. Photobiol. A: Chem. 202 (2009) 92–98.

[214] H. Bodaghi, Y. Mostofi, A. Oromiehie, Z. Zamani, B. Ghanbarzadeh, C. Costa, A. Conte, M.A. Del Nobile, Evaluation of the photocatalytic antimicrobial effects of a TiO2 nanocomposite food packaging film by in vitro and in vivo tests, LWT-Food Science and Technology 50 (2013) 702–706.

[215] H.N. Pham, T. McDowell, E. Wilkins, Photocatalytically-mediated disinfection of water using TiO2 as a catalyst and spore-forming Bacillus pumilus as a model, J. Environ. Sci. Health Part A 30 (1995) 627–636.

[216] Q. Li, Y.W. Li, P. Wu, R. Xie, J.K. Shang, Palladium oxide nanoparticles on nitrogen-Doped titanium oxide: accelerated photocatalytic disinfection and post-Illumination catalytic memory, Adv. Mater. 20 (2008) 3717–3723.

[217] J. Murcia, E. Ávila-Martínez, H. Rojas, J. Navío, M. Hidalgo, Study of the E. coli elimination from urban wastewater over photocatalysts based on metallized TiO2, Appl. Catal. B: Environ. 200 (2017) 469–476.

[218] S. Malato, P. Fernández-Ibáñez, M.I. Maldonado, J. Blanco, W. Gernjak, Decontamination and disinfection of water by solar photocatalysis: recent overview and trends, Catal. Today 147 (2009) 1–59.

[219] U.I. Gaya, A.H. Abdullah, Heterogeneous photocatalytic degradation of organic contaminants over titanium dioxide: a review of fundamentals, progress and problems, J. Photochem. Photobiol. C: Photochem. Rev. 9 (2008) 1–12.

[220] E. Evgenidou, K. Fytianos, I. Poulios, Semiconductor-sensitized photodegradation of dichlorvos in water using TiO2 and ZnO as catalysts, Appl. Catal. B: Environ. 59 (2005) 81–89.

[221] C.M. Ling, A.R. Mohamed, S. Bhatia, Performance of photocatalytic reactors using immobilized TiO2 film for the degradation of phenol and methylene blue dye present in water stream, Chemosphere 57 (2004) 547–554.

[222] C. Tang, V. Chen, The photocatalytic degradation of reactive black 5 using TiO2/UV in an annular photoreactor, Water Res. 38 (2004) 2775–2781.

[223] V. Etacheri, G. Michlits, M.K. Seery, S.J. Hinder, S.C. Pillai, A highly efficient TiO2–xCx nano-heterojunction photocatalyst for visible light induced antibacterial applications, ACS Appl. Mater. Interfaces 5 (2013) 1663–1672.

[224] K. Ouyang, K. Dai, S.L. Walker, Q. Huang, X. Yin, P. Cai, Efficient photocatalytic disinfection of escherichia coli O157: H7 using C70-TiO2 hybrid under visible light irradiation, Sci. Rep. 6 (2016) 25702, http://dx.doi.org/10.1038/srep25702.

[225] J.-K. Shang, P. Wu, R.-C. Xie, Co-doped titanium oxide foam and water disinfection device, U.S. Patent No. 9, 242, 873. 26 Jan. 2016.

[226] C. Hu, J. Guo, Q. Qu, X. Hu, Photocatalytic degradation of pathogenic bacteria with AgI/TiO2 under visible light irradiation, Langmuir 23 (2007) 4982–4987.

[227] Y. Lan, C. Hu, X. Hu, J. Qu, Efficient destruction of pathogenic bacteria with AgBr/TiO2 under visible light irradiation, Appl. Catal. B: Environ. 73 (2007) 354–360.

[228] M.P. Reddy, A. Venugopal, M. Subrahmanyam, Hydroxyapatite-supported Ag–TiO2 as Escherichia coli disinfection photocatalyst, Water Res. 41 (2007) 379–386.

[229] O. Akhavan, M. Abdolahad, Y. Abdi, S. Mohajerzadeh, Synthesis of titania/carbon nanotube heterojunction arrays for photoinactivation of E. coli in visible light irradiation, Carbon 47 (2009) 3280–3287.

[230] V.B. Koli, A.G. Dhodamani, A.V. Raut, N.D. Thorat, S.H. Pawar, S.D. Delekar, Visible light photo-induced antibacterial activity of TiO2-MWCNTs nanocomposites with varying the contents of MWCNTs, J. Photochem. Photobiol. A: Chem. 328 (2016) 50–58.

[231] B. Liu, Y. Xue, J. Zhang, B. Han, J. Zhang, X. Suo, L. Mu, H. Shi, Visible-light-driven TiO2/Ag3PO4 heterostructures with enhanced antifungal activity against agricultural pathogenic fungi Fusarium graminearum and mechanism insight, Environ. Sci. Nano 4 (1) (2017) 255–264.

[232] O. Akhavan, E. Ghaderi, Photocatalytic reduction of graphene oxide nanosheets on TiO2 thin film for photoinactivation of bacteria in solar light irradiation, J. Phys. Chem. C 113 (2009) 20214–20220.

[233] J. Liu, L. Liu, H. Bai, Y. Wang, D.D. Sun, Gram-scale production of graphene oxide–TiO2 nanorod composites: towards high-activity photocatalytic materials, Appl. Catal. B: Environ. 106 (2011) 76–82.

[234] B. Cao, S. Cao, P. Dong, J. Gao, J. Wang, High antibacterial activity of ultrafine TiO2/graphene sheets nanocomposites under visible light irradiation, Mater. Lett. 93 (2013) 349–352.

[235] P. Fernández-Ibáñez, M. Polo-López, S. Malato, S. Wadhwa, J. Hamilton, P. Dunlop, E. D'sa, E. Magee, K. O'shea, D. Dionysiou, Solar photocatalytic disinfection of water using titanium dioxide graphene composites, Chem. Eng. J. 261 (2015) 36–44.

[236] B.R. Cruz-Ortiz, J.W. Hamilton, C. Pablos, L. Díaz-Jiménez, D.A. Cortés-Hernández, P.K. Sharma, M. Castro-Alférez, P. Fernández-Ibañez, P.S. Dunlop, J.A. Byrne, Mechanism of photocatalytic disinfection using titania-graphene composites under UV and visible irradiation, Chem. Eng. J. 316 (2017) 179–186.

[237] W. Bai, V. Krishna, J. Wang, B. Moudgil, B. Koopman, Enhancement of nano titanium dioxide photocatalysis in transparent coatings by polyhydroxy fullerene, Appl. Catal. B: Environ. 125 (2012) 128–135.

[238] S. Rtimi, O. Baghriche, C. Pulgarin, J.-C. Lavanchy, J. Kiwi, Growth of TiO2/Cu films by HiPIMS for accelerated bacterial loss of viability, Surf. Coat. Technol. 232 (2013) 804–813.

[239] S. Rtimi, C. Pulgarin, R. Sanjines, V. Nadtochenko, J.-C. Lavanchy, J. Kiwi, Preparation and mechanism of Cu-decorated TiO2–ZrO2 films showing accelerated bacterial inactivation, ACS Appl. Mater. Interfaces 7 (2015) 12832–12839.

[240] G. Wang, Z. Xing, X. Zeng, C. Feng, D.T. McCarthy, A. Deletic, X. Zhang, Ultrathin titanium oxide nanosheets film with memory bactericidal activity, Nanoscale 8 (2016) 18050–18056.

[241] J. Podporska-Carroll, E. Panaitescu, B. Quilty, L. Wang, L. Menon, S.C. Pillai, Antimicrobial properties of highly efficient photocatalytic TiO2 nanotubes, Appl. Catal. B: Environ. 176 (2015) 70–75.

[242] W. He, H.-K. Kim, W.G. Wamer, D. Melka, J.H. Callahan, J.-J. Yin, Photogenerated charge carriers and reactive oxygen species in ZnO/Au hybrid nanostructures with enhanced photocatalytic and antibacterial activity, J. Am. Chem. Soc. 136 (2013) 750–757.

[243] L. Fisher, S. Ostovapour, P. Kelly, K. Whitehead, K. Cooke, E. Storgårds, J. Verran, Molybdenum doped titanium dioxide photocatalytic coatings for use as hygienic surfaces: the effect of soiling on antimicrobial activity, Biofouling 30 (2014) 911–919.

[244] R. Michal, E. Dworniczek, M. Caplovicova, O. Monfort, P. Lianos, L. Caplovic, G. Plesch, Photocatalytic properties and selective antimicrobial activity of TiO2(Eu)/CuO nanocomposite, Appl. Surf. Sci. 371 (2016) 538–546.

[245] Y. Wang, Y. Wu, H. Yang, X. Xue, Z. Liu, Doping TiO2 with boron or/and cerium elements: effects on photocatalytic antimicrobial activity, Vacuum 131 (2016) 58–64.

[246] M.S. Stan, I.C. Nica, A. Dinischiotu, E. Varzaru, O.G. Iordache, I. Dumitrescu, M. Popa, M.C. Chifiriuc, G.G. Pircalabioru, V. Lazar, Photocatalytic, antimicrobial and biocompatibility features of cotton knit coated with Fe-N-Doped titanium dioxide nanoparticles, Materials 9 (2016) 789.

[247] A. Raut, H. Yadav, A. Gnanamani, S. Pushpavanam, S. Pawar, Synthesis and characterization of chitosan-TiO2: Cu nanocomposite and their enhanced antimicrobial activity with visible light, Colloids Surf. B: Biointerfaces 148 (2016) 566–575.

[248] X. Zeng, Z. Wang, N. Meng, D.T. McCarthy, A. Deletic, J.-H. Pan, X. Zhang, Highly dispersed TiO2 nanocrystals and carbon dots on reduced graphene oxide: ternary nanocomposites for accelerated photocatalytic water disinfection, Appl. Catal. B: Environ. 202 (2017) 33–41.

[249] Q. Zhu, X. Hu, M.S. Stanislaus, N. Zhang, R. Xiao, N. Liu, Y. Yang, A novel P/Ag/Ag2O/Ag3PO4/TiO2 composite film for water purification and antibacterial application under solar light irradiation, Sci. Total Environ. 577 (2017) 236–244.

[250] Y. Ao, J. Xu, D. Fu, X. Shen, C. Yuan, A novel magnetically separable composite photocatalyst: titania-coated magnetic activated carbon, Sep. Purif. Technol. 61 (2008) 436–441.

[251] M. Mangayayam, J. Kiwi, S. Giannakis, C. Pulgarin, I. Zivkovic, A. Magrez, S. Rtimi, FeOx magnetization enhancing E. coli inactivation by orders of magnitude on Ag-TiO2 nanotubes under sunlight, Appl. Catal. B: Environ. 202 (2017) 438–445.

[252] S. Rana, R. Srivastava, M. Sorensson, R. Misra, Synthesis and characterization of nanoparticles with magnetic core and photocatalytic shell: anatase TiO2–NiFe2O4 system, Mater. Sci. Eng.: B 119 (2005) 144–151.

[253] J. Rawat, S. Rana, R. Srivastava, R.D.K. Misra, Antimicrobial activity of composite nanoparticles consisting of titania photocatalytic shell and nickel ferrite magnetic core, Mater. Sci. Eng. C 27 (2007) 540–545.

[254] T.W. Ng, L. Zhang, J. Liu, G. Huang, W. Wang, P.K. Wong, Visible-light-driven photocatalytic inactivation of Escherichia coli by magnetic Fe2O3–AgBr, Water Res. 90 (2016) 111–118.

[255] Y. Chen, K. Liu, Fabrication of magnetically recyclable Ce/N co-doped TiO2/NiFe2O4/diatomite ternary hybrid: improved photocatalytic efficiency under visible light irradiation, J. Alloys Compd. 697 (2017) 161–173.

[256] Y. Yamaguchi, T. Shimodo, N. Chikamori, S. Usuki, Y. Kanai, T. Endo, K.-I. Katsumata, C. Terashima, M. Ikekita, A. Fujishima, Sporicidal performance induced by photocatalytic production of organic peroxide under visible light irradiation, Sci. Rep. Sci. Rep. 6 (2016) 33715, http://dx.doi.org/10.1038/srep33715.

[257] W.F. Yao, X.H. Xu, H. Wang, J.T. Zhou, X.N. Yang, Y. Zhang, S.X. Shang, B.B. Huang, Photocatalytic property of perovskite bismuth titanate, Appl. Catal. B: Environ. 52 (2004) 109–116.

[258] S. Ning, H. Lin, Y. Tong, X. Zhang, Q. Lin, Y. Zhang, J. Long, X. Wang, Dual couples Bi metal depositing and Ag@AgI islanding on BiOI 3D architectures for synergistic bactericidal mechanism of E. coli under visible light, Appl. Catal. B: Environ. 204 (2017) 1–10.

[259] L. Zhang, H. Wang, Z. Chen, P.K. Wong, J. Liu, Bi2WO6 micro/nano-structures: synthesis, modifications and visible-light-driven photocatalytic applications, Appl. Catal. B: Environ. 106 (2011) 1–13.

[260] J. Ren, W. Wang, L. Zhang, J. Chang, S. Hu, Photocatalytic inactivation of bacteria by photocatalyst Bi2WO6 under visible light, Catal. Commun. 10 (2009) 1940–1943.

[261] J. Ren, W. Wang, S. Sun, L. Zhang, J. Chang, Enhanced photocatalytic activity of Bi2WO6 loaded with Ag nanoparticles under visible light irradiation, Appl. Catal. B: Environ. 92 (2009) 50–55.

[262] L.-S. Zhang, K.-H. Wong, H.-Y. Yip, C. Hu, J.C. Yu, C.-Y. Chan, P.-K. Wong, Effective photocatalytic disinfection of E. coli K-12 using AgBr- Ag- Bi2WO6 nanojunction system irradiated by visible light: the role of diffusing hydroxyl radicals, Environ. Sci. Technol. 44 (2010) 1392–1398.

[263] S.O. Alfaro, A. Martínez-de la Cruz, L.M. Torres-Martínez, S. Lee, Remove of marine plankton by photocatalysts with Aurivillius-type structure, Catal. Commun. 11 (2010) 326–330.

[264] F. Qin, H. Zhao, G. Li, H. Yang, J. Li, R. Wang, Y. Liu, J. Hu, H. Sun, R. Chen, Size-tunable fabrication of multifunctional Bi2O3 porous nanospheres for photo-catalysis, bacteria inactivation and template-synthesis, Nanoscale 6 (2014) 5402–5409.

[265] W. Wang, X. Chen, G. Liu, Z. Shen, D. Xia, P.K. Wong, C.Y. Jimmy, Monoclinic

dibismuth tetraoxide: a new visible-light-driven photocatalyst for environmental remediation, Appl. Catal. B: Environ. 176 (2015) 444–453.

[266] D. Wu, B. Wang, W. Wang, T. An, G. Li, T.W. Ng, H.Y. Yip, C. Xiong, H.K. Lee, P.K. Wong, Visible-light-driven BiOBr nanosheets for highly facet-dependent photocatalytic inactivation of Escherichia coli, J. Mater. Chem. A 3 (2015) 15148–15155.

[267] T.S. Jamil, E.S. Mansor, M.A. El-Liethy, Photocatalytic inactivation of E. coli using nano-size bismuth oxyiodide photocatalysts under visible light, J. Environ. Chem. Eng. 3 (2015) 2463–2471.

[268] Y. Long, Y. Wang, D. Zhang, P. Ju, Y. Sun, Facile synthesis of BiOI in hierarchical nanostructure preparation and its photocatalytic application to organic dye removal and biocidal effect of bacteria, J. Colloid Interface Sci. 481 (2016) 47–56.

[269] J. Liang, J. Deng, M. Li, T. Xu, M. Tong, Bactericidal activity and mechanism of Ti-doped BiOI microspheres under visible light irradiation, Colloids Surf. B: Biointerfaces 147 (2016) 307–314.

[270] Y. Wang, L. Lin, F. Li, L. Chen, D. Chen, C. Yang, M. Huang, Enhanced photocatalytic bacteriostatic activity towards Escherichia coli using 3D hierarchical microsphere BiOI/BiOBr under visible light irradiation, Photochem. Photobiol. Sci. 15 (2016) 666–672.

[271] C. Adán, J. Marugán, S. Obregón, G. Colón, Photocatalytic activity of bismuth vanadates under UV-A and visible light irradiation: inactivation of Escherichia coli vs oxidation of methanol, Catal. Today 240 (2015) 93–99.

[272] Y. Park, K.J. McDonald, K.-S. Choi, Progress in bismuth vanadate photoanodes for use in solar water oxidation, Chem. Soc. Rev. 42 (2013) 2321–2337.

[273] W. Wang, Y. Yu, T. An, G. Li, H.Y. Yip, J.C. Yu, P.K. Wong, Visible-light-driven photocatalytic inactivation of E. coli K-12 by bismuth vanadate nanotubes: bactericidal performance and mechanism, Environ. Sci. Technol. 46 (2012) 4599–4606.

[274] Z. Xiang, Y. Wang, D. Zhang, P. Ju, BiOI/BiVO4 p-n heterojunction with enhanced photocatalytic activity under visible-light irradiation, J. Ind. Eng. Chem. 40 (2016) 83–92.

[275] C. Adán, J. Marugán, S. Obregón, G. Colón, Photocatalytic Escherichia coli inactivation by means of trivalent Er3+, Y3+ doping of BiVO4 system, Appl. Catal. A: Gen. 526 (2016) 126–131.

[276] C.-K. Huang, T. Wu, C.-W. Huang, C.-Y. Lai, M.-Y. Wu, Y.-W. Lin, Enhanced photocatalytic performance of BiVO4 in aqueous AgNO3 solution under visible light irradiation, Appl. Surf. Sci. 399 (2017) 10–19.

[277] H. Gan, G. Zhang, H. Huang, Enhanced visible-light-driven photocatalytic inactivation of Escherichia coli by Bi2O2CO3/Bi3NbO7 composites, J. Hazard. Mater. 250 (2013) 131–137.

[278] Y.-S. Xu, Z.-J. Zhang, W.-D. Zhang, Facile preparation of heterostructured Bi2O3/Bi2MoO6 hollow microspheres with enhanced visible-light-driven photocatalytic and antimicrobial activity, Mater. Res. Bull. 48 (2013) 1420–1427.

[279] Y.-S. Xu, Y.-X. Yu, W.-D. Zhang, Wide bandgap Bi2O2CO3-coupled Bi2MoO6 heterostructured hollow microspheres: one-pot synthesis and enhanced visible-light photocatalytic activity, J. Nanosci. Nanotechnol. 14 (2014) 6800–6808.

[280] S. Dervin, D.D. Dionysiou, S.C. Pillai, 2D nanostructures for water purification: graphene and beyond, Nanoscale 8 (2016) 15115–15131.

[281] D. Xia, T. An, G. Li, W. Wang, H. Zhao, P.K. Wong, Synergistic photocatalytic inactivation mechanisms of bacteria by graphene sheets grafted plasmonic Ag AgX (X = Cl, Br I) composite photocatalyst under visible light irradiation, Water Res. 99 (2016) 149–161.

[282] N. Khadgi, A.R. Upreti, Y. Li, Simultaneous bacterial inactivation and degradation of an emerging pollutant under visible light by ZnFe2O4 co-modified with Ag and rGO, RSC Adv. 7 (2017) 27007–27016.

[283] C. Liu, D. Kong, P.-C. Hsu, H. Yuan, H.-W. Lee, Y. Liu, H. Wang, S. Wang, K. Yan, D. Lin, Rapid water disinfection using vertically aligned MoS2 nanofilms and visible light, Nat. Nanotechnol.

[284] S. Rtimi, A. Gulin, R. Sanjines, C. Pulgarin, V. Nadtochenko, J. Kiwi, Innovative self-sterilizing transparent Fe?phosphate polyethylene films under visible light, RSC Adv. 6 (2016) 77066–77074.

[285] A. Fujishima, Electrochemical photolysis of water at a semiconductor electrode, Nature 238 (1972) 37–38.

[286] Z. He, J. Fu, B. Cheng, J. Yu, S. Cao, Cu2(OH)2 CO3 clusters: novel noble-metal-free cocatalysts for efficient photocatalytic hydrogen production from water splitting, Appl. Catal. B: Environ. 205 (2017) 104–111.

[287] M. Ni, M.K. Leung, D.Y. Leung, K. Sumathy, A review and recent developments in photocatalytic water-splitting using TiO2 for hydrogen production, Renew. Sustain. Energy Rev. 11 (2007) 401–425.

[288] S. Banerjee, D.D. Dionysiou, S.C. Pillai, Self-cleaning applications of TiO2 by photo-induced hydrophilicity and photocatalysis, Appl. Catal. B: Environ. 176 (2015) 396–428.

[289] A. Mills, S.-K. Lee, A web-based overview of semiconductor photochemistry-based current commercial applications, J. Photochem. Photobiol. A: Chem. 152 (2002) 233–247.

[290] J. Yu, X. Zhao, C.Y. Jimmy, G. Zhong, J. Han, Q. Zhao, The grain size and surface hydroxyl content of super-hydrophilic TiO2/SiO2 composite nanometer thin films, J. Mater. Sci. Lett. 20 (2001) 1745–1748.

[291] Y. Hendrix, A. Lazaro, Q. Yu, J. Brouwers, Titania-Silica composites a review on the photocatalytic activity and synthesis methods, World J. Nano Sci. Eng. 5 (2015) 161.

[292] http://www.thomasnet.com/products/antimicrobial-coatings-97002182-1.html (last accessed on 06/10/2017).

[293] S. Ferraris, Smart Composite Coatings and Membranes, (2016).

[294] http://www.tipe.com.cn/index.php/solutions/anti-microbial (last accessed on 06/10/2017).

[295] http://corporate.evonik.com/en/products/industry-teams/construction/pages/additives.aspx (last accessed on 06/10/2017).

[296] http://www.taiyo-europe.com/fileadmin/user_upload/downloads/Taiyo_Kogyo_Group_Technology.pdf (last accessed on 06/10/2017).

[297] http://www.greenearthnanoscience.com/press-releases-sick-building.php (last accessed on 06/10/2017).

[298] http://www.nanotech-now.com/columns/?article=636 (last accessed on 06/10/2017).

[299] http://www.agrob-buchtal.de/en/cd/produkte/produkte_fiz_uebersicht.html?pe_id=90 (last accessed on 06/10/2017).

[300] http://nanomagic.ie/(last accessed on 06/10/2017).

[301] http://www.kastus.com(last accessed on 06/10/2017).

[302] S.L. Markov, A.M. Vidaković, Testing methods for antimicrobial activity of TiO2 photocatalyst, Acta Period. Technol. (2014) 141–152.

[303] A. Mills, C. Hill, P.K. Robertson, Overview of the current ISO tests for photocatalytic materials, J. Photochem. Photobiol. A: Chem. 237 (2012) 7–23.

[304] N.S. Leyland, J. Podporska-Carroll, J. Browne, S.J. Hinder, B. Quilty, S.C. Pillai, Highly Efficient F, Cu doped TiO2 anti-bacterial visible light active photocatalytic coatings to combat hospital-acquired infections, Sci. Rep. 6 (2016) 24770, http://dx.doi.org/10.1038/srep24770.

[305] L. Kubáč, J. Akrman, K. Kejlová, H. Bendová, K. Klánová, Z. Hladíková, P. Pikal, L. Kovaříková, L. Kašparová, D. Jírová, Characteristics of titanium dioxide microdispersions with different photo-activity suitable for sunscreen formulations, Int. J. Pharm. 481 (2015) 91–96.

[306] R. Sadowski, M. Strus, M. Buchalska, P.B. Heczko, W. Macyk, Visible light induced photocatalytic inactivation of bacteria by modified titanium dioxide films on organic polymers, Photochem. Photobiol. Sci. 14 (2015) 514–519.

[307] Y. Yao, T. Ochiai, H. Ishiguro, R. Nakano, Y. Kubota, Antibacterial performance of a novel photocatalytic-coated cordierite foam for use in air cleaners, Appl. Catal. B: Environ. 106 (2011) 592–599.

[308] H. Foster, D. Sheel, P. Sheel, P. Evans, S. Varghese, N. Rutschke, H. Yates, Antimicrobial activity of titania/silver and titania/copper films prepared by CVD, J. Photochem. Photobiol. A: Chem. 216 (2010) 283–289.

[309] P. Magalhães, J. Ângelo, V.M. Sousa, O.C. Nunes, L. Andrade, A. Mendes, Synthesis and assessment of a graphene-based composite photocatalyst, Biochem. Eng. J. 104 (2015) 20–26.

[310] S.P. Tallósy, L. Janovák, J. Ménesi, E. Nagy, Á. Juhász, L. Balázs I. Deme, N. Buzás, I. Dékány, Investigation of the antibacterial effects of silver-modified TiO2 and ZnO plasmonic photocatalysts embedded in polymer thin films, Environ. Sci. Pollut. Res. 21 (2014) 11155–11167.

[311] H. Ishiguro, R. Nakano, Y. Yao, J. Kajioka, A. Fujishima, K. Sunada, M. Minoshima, K. Hashimoto, Y. Kubota, Photocatalytic inactivation of bacteriophages by TiO2-coated glass plates under low-intensity, long-wavelength UV irradiation, Photochem. Photobiol. Sci. 10 (2011) 1825–1829.

[312] J. Krýsa, E. Musilová, J. Zita, Critical assessment of suitable methods used for determination of antibacterial properties at photocatalytic surfaces, J. Hazard. Mater. 195 (2011) 100–106.

[313] R. Nakano, H. Ishiguro, Y. Yao, J. Kajioka, A. Fujishima, K. Sunada, M. Minoshima, K. Hashimoto, Y. Kubota, Photocatalytic inactivation of influenza virus by titanium dioxide thin film, Photochem. Photobiol. Sci. 11 (2012) 1293–1298.

[314] H. Ando, N. Kawasaki, N. Yamano, K. Uegaki, A. Nakayama, Biodegradation of a poly (ε-caprolactone-co-l-lactide)?visible-light-sensitive TiO2 composite with an on/off biodegradation function, Polym. Degrad. Stab. 114 (2015) 65–71.

[315] S.P. Tallósy, L. Janovák, E. Nagy, Á. Deák, Á. Juhász, E. Csapó, N. Buzás, I. Dékány, Adhesion and inactivation of Gram-negative and Gram-positive bacteria on photoreactive TiO2/polymer and Ag–TiO2/polymer nanohybrid films, Appl. Surf. Sci. 371 (2016) 139–150.

[316] G.F. Samu, Á. Veres, S.P. Tallósy, L. Janovák, I. Dékány, A. Yepez, R. Luque, C. Janáky, Photocatalytic, photoelectrochemical and antibacterial activity of benign-by-design mechanochemically synthesized metal oxide nanomaterials, Catal. Today 284 (2017) 3–10.

[317] http://zibajp.com/H.G/HG_Downloads/Antimicrobial%20products-Test%20for%20antimicrobial%20activity%20and%20efficacy.pdf (last accessed on 06/10/2017).

[318] H.W. Swofford, An overview of antimicrobial testing for textile applications, AATCC review 6 (2010) 51–55.

[319] http://www.jfrl.or.jp/item/effecttest/jis-r-1702.html (last accessed on 06/10/2017).

[320] L. Jis, Testing for Antibacterial Activity and Efficacy on Textile Products, (2002), p. 1902.

[321] E. Pinho, L. Magalhães, M. Henriques, R. Oliveira, Antimicrobial activity assessment of textiles: standard methods comparison, Annals of Microbiology 61 (2011) 493–498.

[322] Z. JIS, 2801. 2000, Antimicrobial products–test for antimicrobial activity and efficacy. Japanese Industrial Standard, (2000).

[323] Z. JIS, 2801. 2000 Antimicrobial products–Test for antimicrobial activity and efficacy, Japanese Standards Association: Akasaka, Minato-ku, Japan, (2000).

[324] http://kikakurui.com/r1/R1702-2012-01.html (last accessed on 06/10/2017).